General Disclaimer

One or more of the Following Statements may affect this Document

- This document has been reproduced from the best copy furnished by the organizational source. It is being released in the interest of making available as much information as possible.

- This document may contain data, which exceeds the sheet parameters. It was furnished in this condition by the organizational source and is the best copy available.

- This document may contain tone-on-tone or color graphs, charts and/or pictures, which have been reproduced in black and white.

- This document is paginated as submitted by the original source.

- Portions of this document are not fully legible due to the historical nature of some of the material. However, it is the best reproduction available from the original submission.

Produced by the NASA Center for Aerospace Information (CASI)

NASW-3646
SCOSTEP (144)

Middle Atmosphere Program

(NASA-CR-175478) MIDDLE ATMOSPHERE PROGRAM. HANDBOOK FOR MAP, VOLUME 8 (International Council of Scientific Unions) 79 p HC A05/MF A01; also available from SCOSTEP CSCI 04A G3/42
N85-20445 THRU N85-20449 Unclas 18261

HANDBOOK FOR MAP

Volume 8

Edited by
C. F. Sechrist, Jr.

M I D D L E

A T M O S P H E R E

P R O G R A M

HANDBOOK FOR MAP

VOLUME 8

Edited by

C. F. Sechrist, Jr.
Chairman
MAP Publications Committee

July 1983

Published for the ICSU Scientific Committee on Solar-Terrestrial Physics (SCOSTEP) with financial assistance in part from Unesco Subvention 1981-1983 DG/7.6.2/Sub. 13 (SC) and in part from the National Aeronautics and Space Administration Contract NASW 3646.

Copies available from SCOSTEP Secretariat, University of Illinois, 1406 W. Green Street, Urbana, Illinois 61801

CONTENTS

PART 1 MAP PROJECT REPORTS 1

PART 2 MAP STUDY GROUP REPORT 53

PART 3 NATIONAL REPORT 75

PRECEDING PAGE BLANK NOT FILMED

N85-20446

THE FIRST WINTER OF MAP - DYNAMICS, 1982/83: A WINTER WITH THREE DIFFERENT WARMING PERIODS

Barbara Naujokat, Karin Petzoldt, Karin Labitzke, and Renate Lenschow

ABSTRACT

A synoptic description is given for the first winter of MAP-Dynamics, 1982/83. After a cold early winter period three warming periods were observed at the end of December, the end of January, and the end of February. In March a pronounced late winter cooling occurred in the upper stratosphere, whereas in the lower levels the final warming started slowly, but was not accomplished before mid-April.

The momentum budget, calculated from the daily height and temperature charts, is discussed in terms of the divergence of the Eliassen-Palm-Vector in the second part of this report.

1. SYNOPTIC DESCRIPTION

(a) The Early Winter

The winter 1982/83 started with the development of an extremely strong and cold polar vortex in the lower stratosphere during November and December, but at higher levels the circulation changed to normal winter conditions and even to a slightly disturbed pattern in the upper stratosphere. The march of radiances and temperatures over the North Pole (Figure 1) demonstrates this with values above the long-term mean at channel 27 (maximum weight around 1.7 mbar) of the SSU (Stratospheric Sounding Unit),with quite normal values at channel 26 (maximum weight around 4 mbar) and at the 10-mbar level, and with values well below the long-term mean at the 30-mbar level.

In spite of a relatively strong development of height wave 1 (amplitudes of height and temperature waves 1 and 2 at 30 mbar, at 60°N, are shown in Figure 2e and 2b) in the beginning of December, no significant Canadian warming could be observed in contrary to the year before (see Beilage SO 9/82B). The eddy heat transport northward by this wave at 30 mbar (Figure 9) was not as strong as in December 1981. Thus, there was only a small peak in the march of temperatures over the North Pole (Figure 1b), the temperature gradient between 60°N and the pole was not reversed (Figure 2d) and the mean zonal wind at 60°N (Figure 2a) decelerated only by a small amount.

In the following time the lower stratosphere again continuously cooled and a first wintertime minimum of temperature was reached on 22 December (Figure 1b and 3). The 10-mbar chart of this day shows a cold polar vortex over the Siberian arctic surrounded by strong westerly winds, which reached its first maximum of this winter in the zonal mean of 60°N around this time (Figure 2a and 3).

(b) The First Warming Period

At the end of December the first warming pulse occurred, when for the first time a strong geopotential flux upwards through 30 mbar, at 60°N, (Figure 2c) was observed. At the same time the height waves 1 and 2 showed a relatively big amplitude at 30 mbar (Figure 2e) and eddy heat was transported northwards by both waves, (Figure 9). However, the warming was mainly confined to the upper stratospheric levels and did not propagate much downward in the following days. The radiances and temperatures over the North Pole (Figure 1a and 1b) considerably increased, but the peak value at 30 mbar was still below the

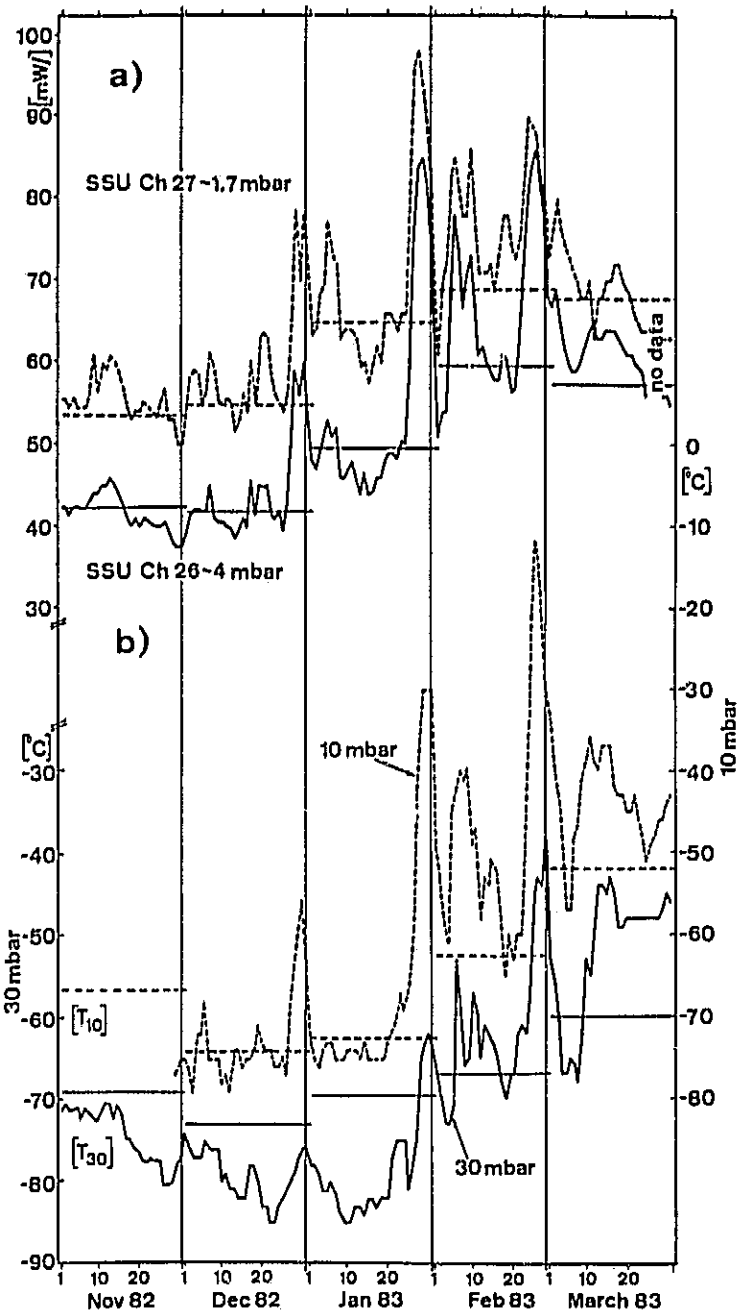

Figure 1. March of radiances and temperatures over the North Pole: (horizontal lines are long-term monthly means). a) Radiances [mW/m^{2}sr cm^{-1}] of channel 27 and 26 are the SSU, max. weight around 1.7 and 4 mbar (courtesy Meteorological Office Bracknell, UK). b) Temperatures [°C] at 10 and 30 mbar.

long-term mean of December and also at 10 mbar no temperature gradient reversal between 60°N and the pole was attained (Figure 2d). At higher levels the warming was well documented by all available data. The lidar data measured over Haute Provence, France indicated a warm stratopause around 45 km, and the time-height section of rocketsonde observations over Heiss Island, USSR (Figure 5) show the warmed region which descended to about this height in the beginning of January. A warm center was established over the polar region as can be seen in Figure 11, showing the radiances at channel 27 (maximum weight around 1.7 mbar) of the SSU on 5 January. This temperature gradient reversal persisted until mid-January. Wind measurements at mesospheric levels and at the mesopause region (Figure 6) indicate, moreover, a short-lived circulation reversal at these heights. Over middle and western Europe (Collm and Sheffield) a disturbed wind field was observed with weak easterlies during two days, and over Canada (Saskatoon) the westerly wind became erratic with two reversal periods at the end of December and the beginning of January. In contrary, at lower levels the mean zonal wind at 60°N (Figure 2a) only weakened and at 30 mbar almost no effect is discernible (see also Figure 3). With an amplified height wave 2 (Figure 2e) in the beginning of January eddy momentum was transported northwards (Figure 9) and the westerly mean zonal wind reached an absolute maximum at latitudes between 60°N and 70°N around 10 January (Figure 2a and 3). The value of 55 m/s lies 10 m/s above the value so far observed since the winter 1965/66, as catalogued by LABITZKE AND GORETZKI (1982).

(c) The Second Warming Period

Starting with 10 January, the day of strongest westerly wind, the amplitude of height wave 1 strengthened and developed into the maximum of this winter on 23 January (Figure 2e). At this time some of the lowest temperatures ever observed at the 30-mbar level occurred over northern Europe, where the northern hemispheric center of the cold air was displaced to. Temperature values of about -90°C at 30 mbar, as documented by several radiosonde stations over Scotland and Norway (Figure 4) have been observed up to this date only in February 1980 when an extremely cold polar vortex preceded a major stratospheric warming. It is interesting to note that the cold lower stratosphere (Figure 4) was connected with a very warm troposphere. Moreover, the radiosonde observation over Berlin, FRG (Figure 4) already indicated the warming of the upper stratosphere and the lidar measurements over Haute Provence, France (Figure 4) as well as the rocket observations over Heiss Island, USSR (Figure 5) confirmed this warming and beyond that demonstrated the related mesospheric cooling. Infrared measurements over Kjeller, Norway also yielded low temperatures of about -70°C at about 85 km height.

Concurrent with the amplification of height wave 1 the amplitude of height wave 2 decreased (Figure 2e), the geopotential flux upwards through 30 mbar steadily increased until 26 January (Figure 2c), and the eddy heat transport was strongly directed northwards (Figure 9). A major warming, i.e., a circulation break-down seemed to be possible. The 10-mbar chart and the chart of radiances at channel 27 (around 1.7 mbar) of the SSU (Figure 7) show a pronounced warm region over Asia with the axis tilted westwards as height increases and the cold air displaced towards Europe and Canada, respectively - thus showing the strong amplitude of temperature wave 1 which is plotted for the 30-mbar level in Figure 2b. At the end of January the radiances and temperatures over the North Pole (Figure 1) reached the second peak of this winter and the temperature gradient between 60°N and the pole was reversed down to 10 mbar (Figure 2d). After a short time of cooling a second warming pulse occurred during the first ten days of February (Figure 1), leading now a temperature gradient reversal at 30 mbar, too (Figure 2d). The two pulses of this warming period can also be seen at the time-height section of rocket-sonde temperatures over Heiss Island (Figure 5) with the first pulse exhibiting higher temperature values but the second one penetrating deeper into the lower stratosphere. A similar behavior was observed with the lidar over Haute Provence.

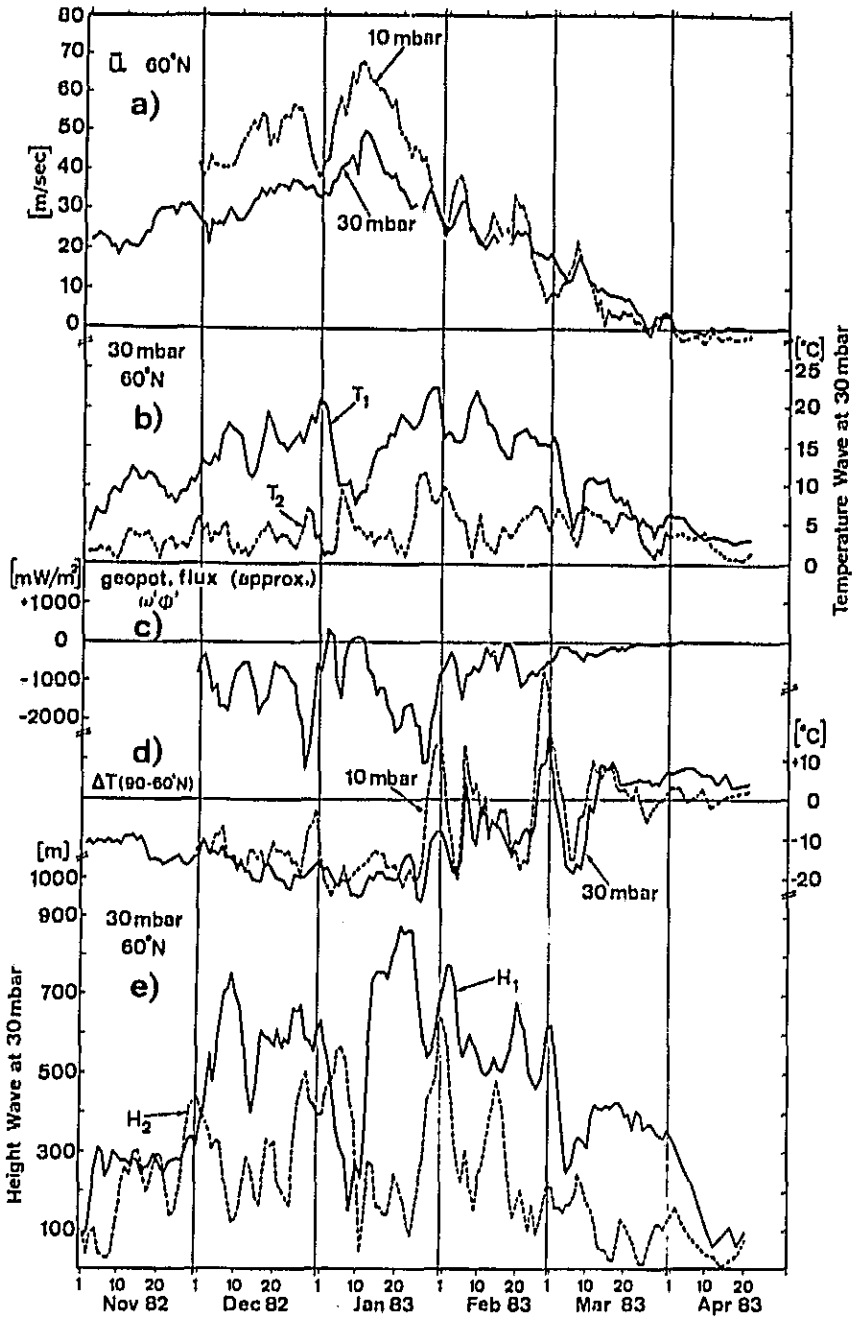

Figure 2. Derived quantities (daily values) describing the winter 1982/83:
a) Mean zonal wind [m s^{-1}] at 60°N, 10 and 30 mbar
b) Amplitudes of temperature waves 1 and 2 [°C] at 60°N, 30 mbar
c) Geopotential flux [mW m^{-2}] through 30 mbar at 60°N
d) Temperature differences [°C] between North Pole and 60°N, 10 and 30 mbar.

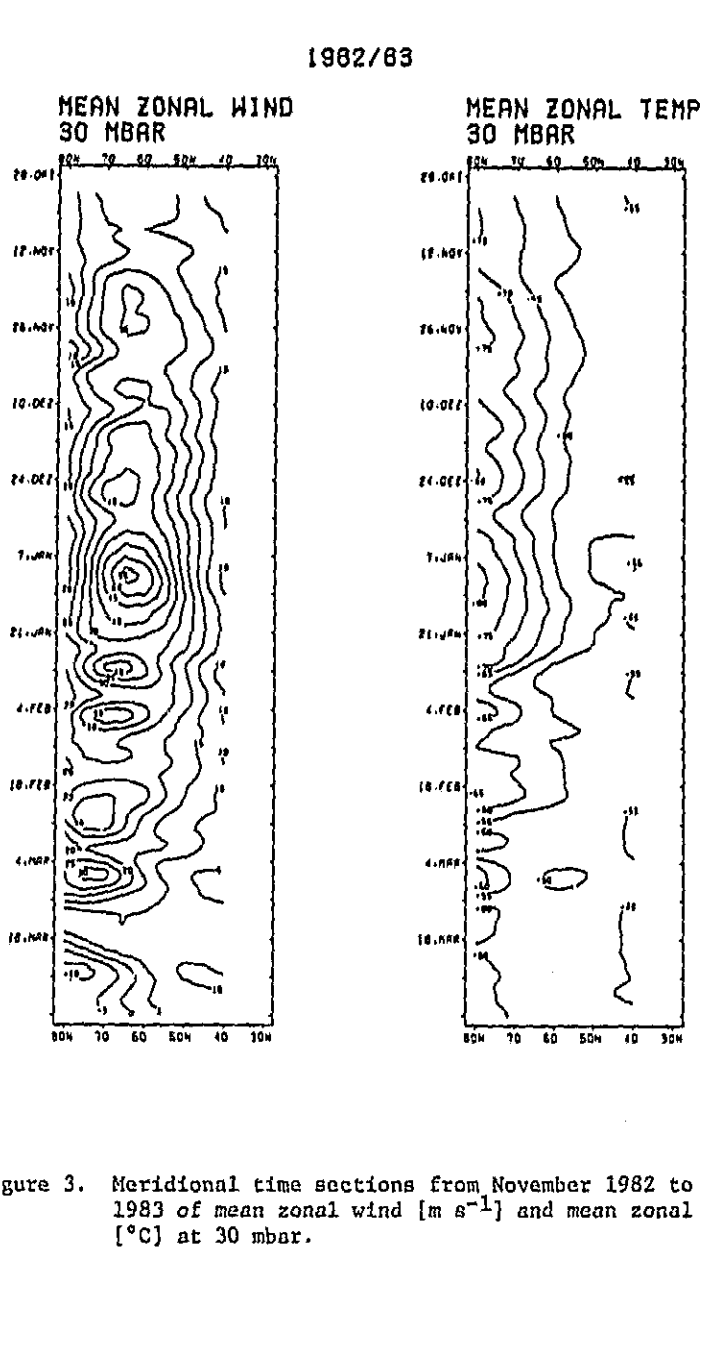

Figure 3. Meridional time sections from November 1982 to March 1983 of mean zonal wind [m s^{-1}] and mean zonal temperature [°C] at 30 mbar.

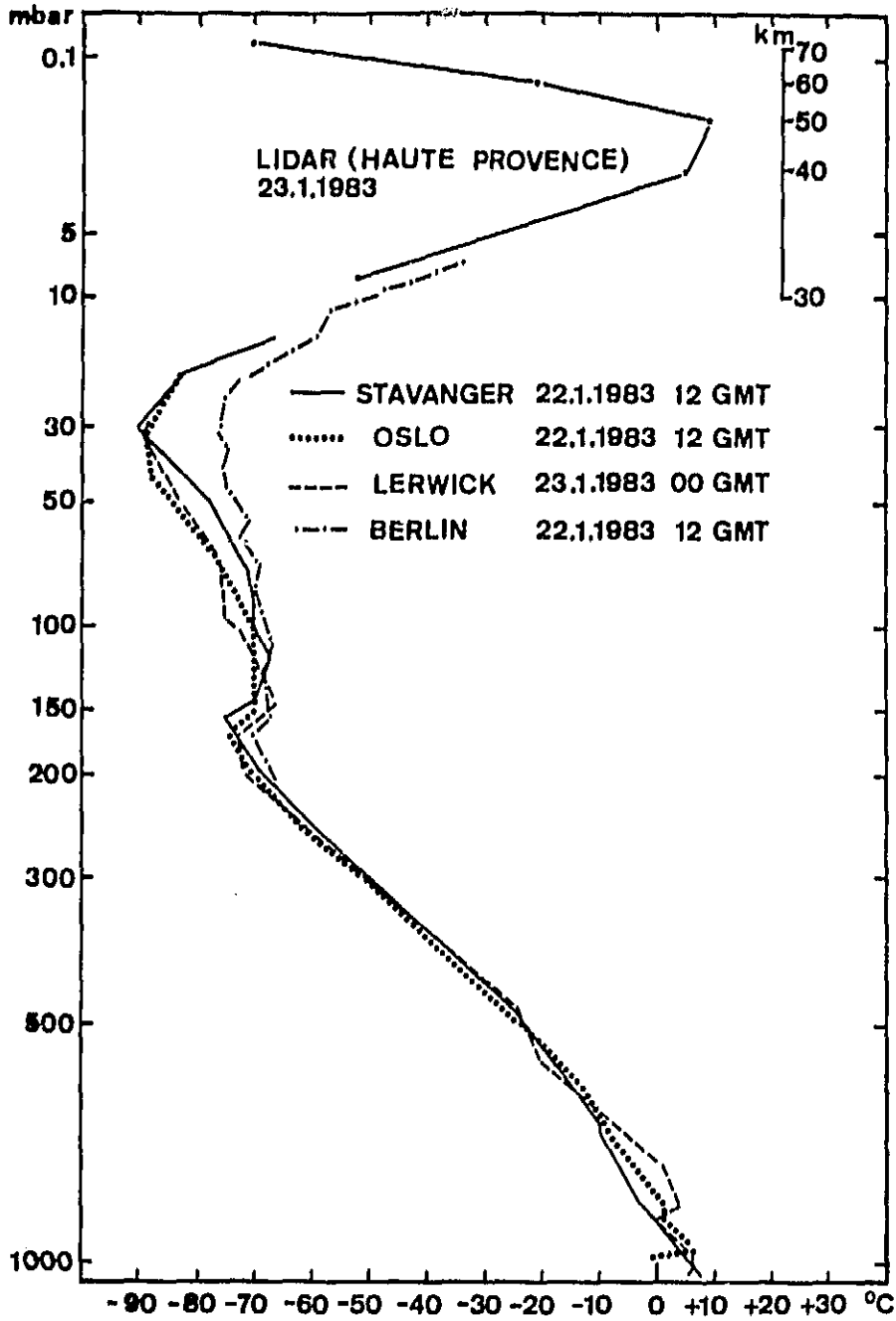

Figure 4. Radiosonde ascents at several stations over Europe on 22/23 January and lidar observation over Haute Provence (courtesy Service d'Aeronomie, Verrieres-le-Buisson, France).

However, no break-down of the polar vortex was attained. The mean zonal wind at 60°N (Figure 2a and 3), already decreasing since 10 January when eddy momentum was transported southwards by the developing height wave 1 (Figure 9), did not reach negative values. As can be seen in Figure 9 the eddy momentum transport by wave 1 changed to be strongly directed northwards at the 30-mbar level from about 23 January to 5 February, while a weaker southward transport occurred by an amplified height wave 2 around 1 February (see also Figure 2e). The momentum budget is discussed in terms of the divergence of the Eliassen-Palm-Vector in section 2.

(d) The Third Warming Period

There was only a short time of cooling before the third period of warming started at the end of February, when again a strong northward eddy heat transport by wave 1 occurred at 30 mbar (Figure 9). The 10-mbar chart and the chart of radiances at channel 27 (around 1.7 mbar) of the SSU (Figure 7) of 23 February show a very similar temperature distribution to that of 26 January, although the radiances did not reach the same high values. The march of radiances and temperatures over the North Pole (Figure 1) also shows that the warming was much stronger than before at lower and middle stratospheric levels, but not at the upper stratosphere. This was confirmed by the lidar observations over Haute Provence and by the rocketsonde observations over Heiss Island (Figure 5). At mesospheric heights the warm center shifted towards the south as height increases, as can be seen by the temperature charts retrieved from the measurements of the SAMS (Stratospheric and Mesospheric Sounder) for 27 February (Figure 8). It must be noticed that these measurements are terminated at the polar cap so that the broken lines over the polar region are somewhat arbitrary. Especially the cold center over the pole at the 0.03-mbar level should probably be much stronger, as indicated by the very low temperatures at these heights over Heiss Island (Figure 5).

However, the temperature gradient between 60°N and the North Pole was reversed throughout the stratosphere (for 30 and 10 mbar see Figure 2d), the mean zonal wind decreased at stratospheric levels (Figure 2a and 3) and reached negative values at mesospheric levels over middle Europe as well as over Canada (Figure 6). Thus an early final warming could be expected.

(e) The Late Winter Cooling

However, a temporary cooling in the beginning of March with an increase of the mean zonal wind at 60°N (Figures 1, 2a, 2d and 3) was followed by a very slow progress of the spring reversal in the lower stratosphere and a pronounced late winter cooling in the upper stratosphere. Although the temperature gradient between 60°N and the pole (Figure 2d) was reversed since 10 March in the middle stratosphere and a continuously southward directed eddy momentum transport occurred during March (Figure 9), the mean zonal wind at 60°N (Figure 2a) remained weakly from the west until the end of the month and still fluctuated around zero during the whole of April.

Accordingly, the 10-mbar chart of 31 March show only a weak anticyclone over the polar region. For the same day the chart of radiances at channel 27 (around 1.7 mbar) of the SSU (Figure 7) show the cold air of the upper stratosphere centered over the pole. At mesospheric heights (Figure 6) strong westerly zonal winds were observed over Canada and middle Europe, reaching the highest values of this winter at about 95 km before the onset of the spring anomaly at the end of March.

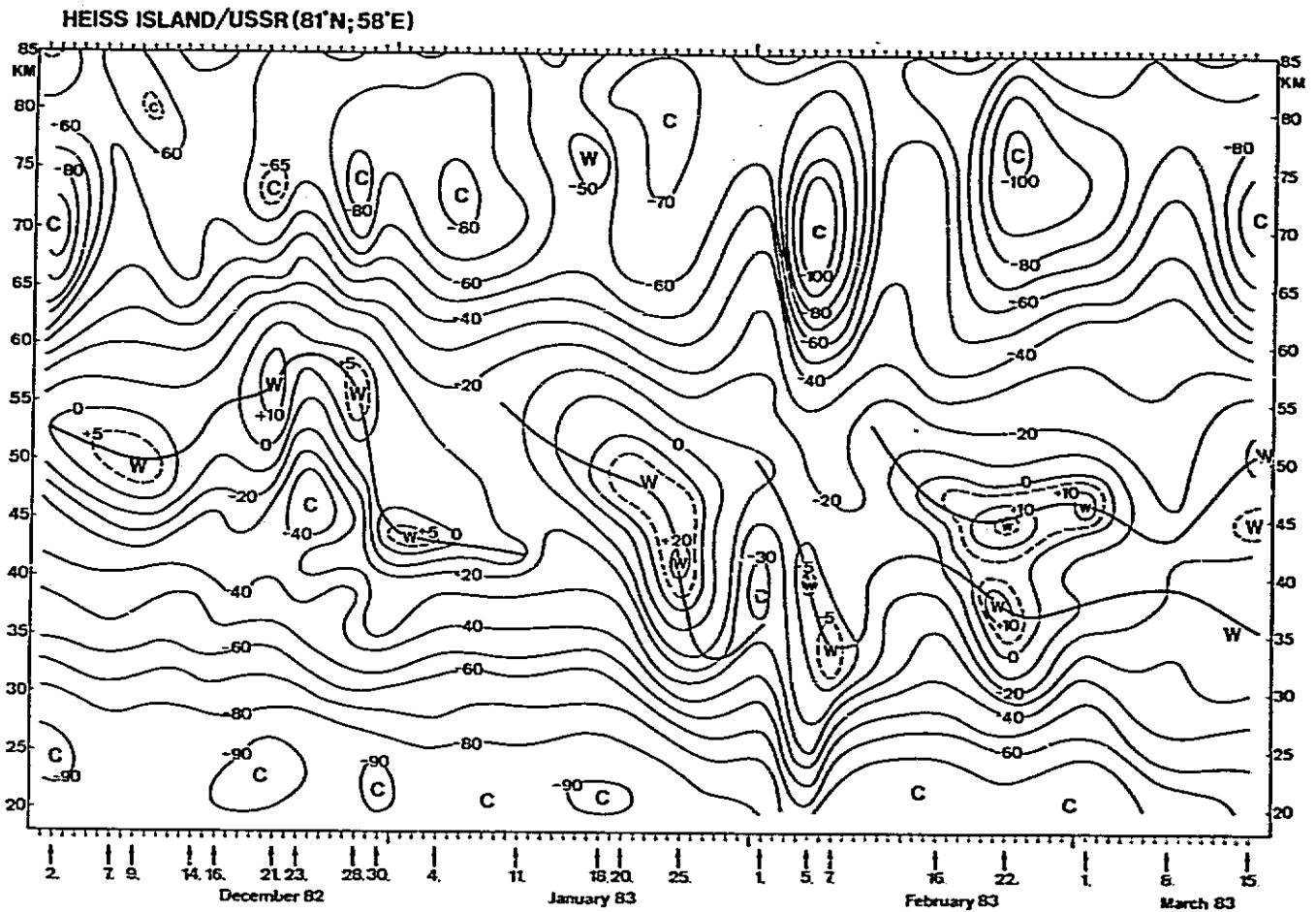

Figure 5. Time height section of rocketsonde temperatures [°C] from 2 December 1982 to 15 March 1983.

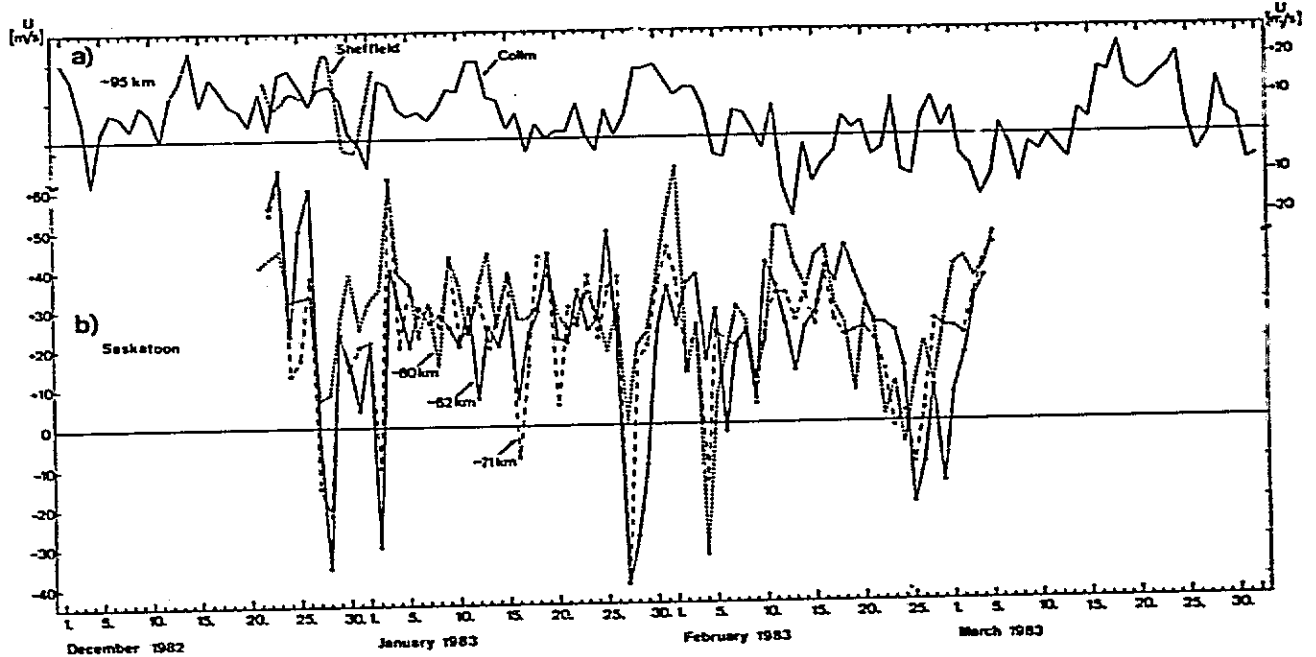

Figure 6. a) Prevailing zonal winds [m s^{-1}] around 95 km over middle (51 N, 13 E) and Western (53 N, 2 W) Europe measured by low frequency ion drift (courtesy Geophysical Observatory Collm, GDR), and by meteor radar (courtesy Physical Department, University Sheffield, UK), respectively. b) Zonal winds [m s^{-1}] over Canada (52 N, 107 W) at three layers (58-66 km layer and 67-75 km layer daily means, 76-84 km layer tidally corrected) measured by partial-reflection radar (courtesy University Saskatchewan, Saskatoon, Canada).

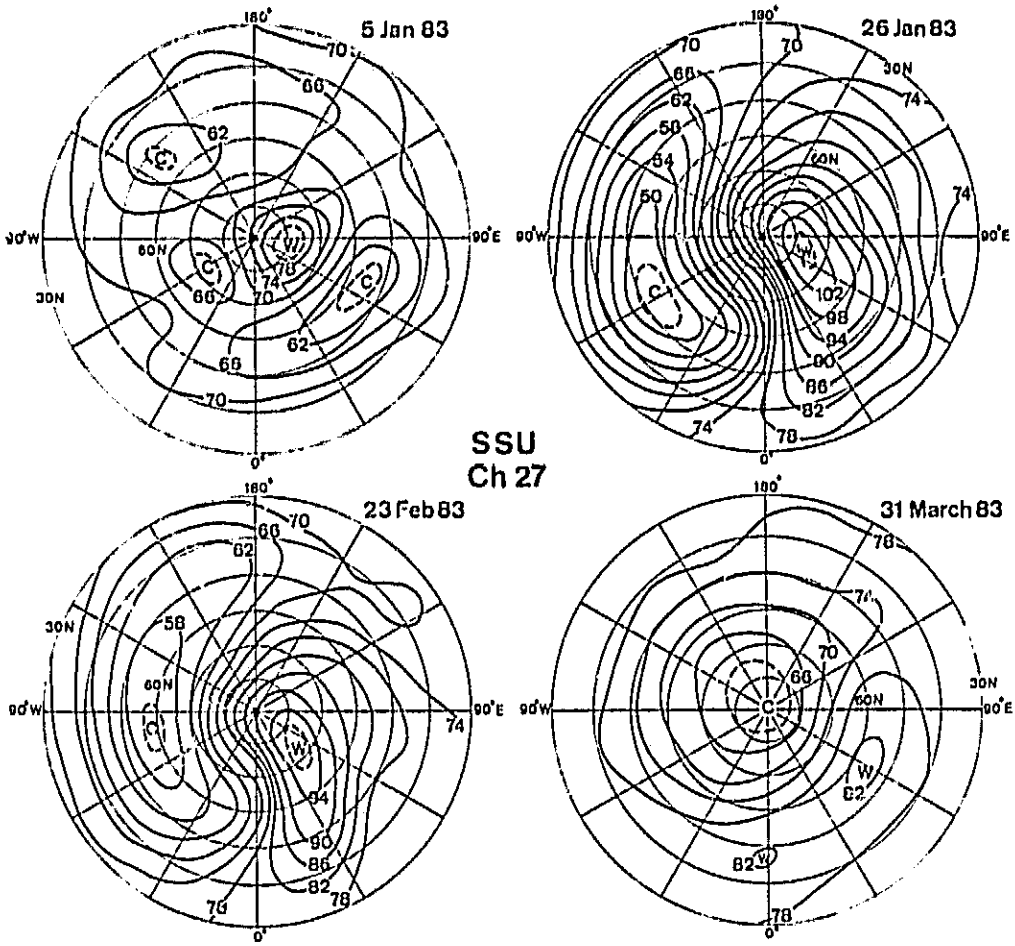

Figure 7. Charts of radiances [$mW/m^2 sr\ cm^{-1}$] at channel 27 of the SSU, maximum weight around 1.7 mbar (courtesy Meteorological Office Bracknell, UK).

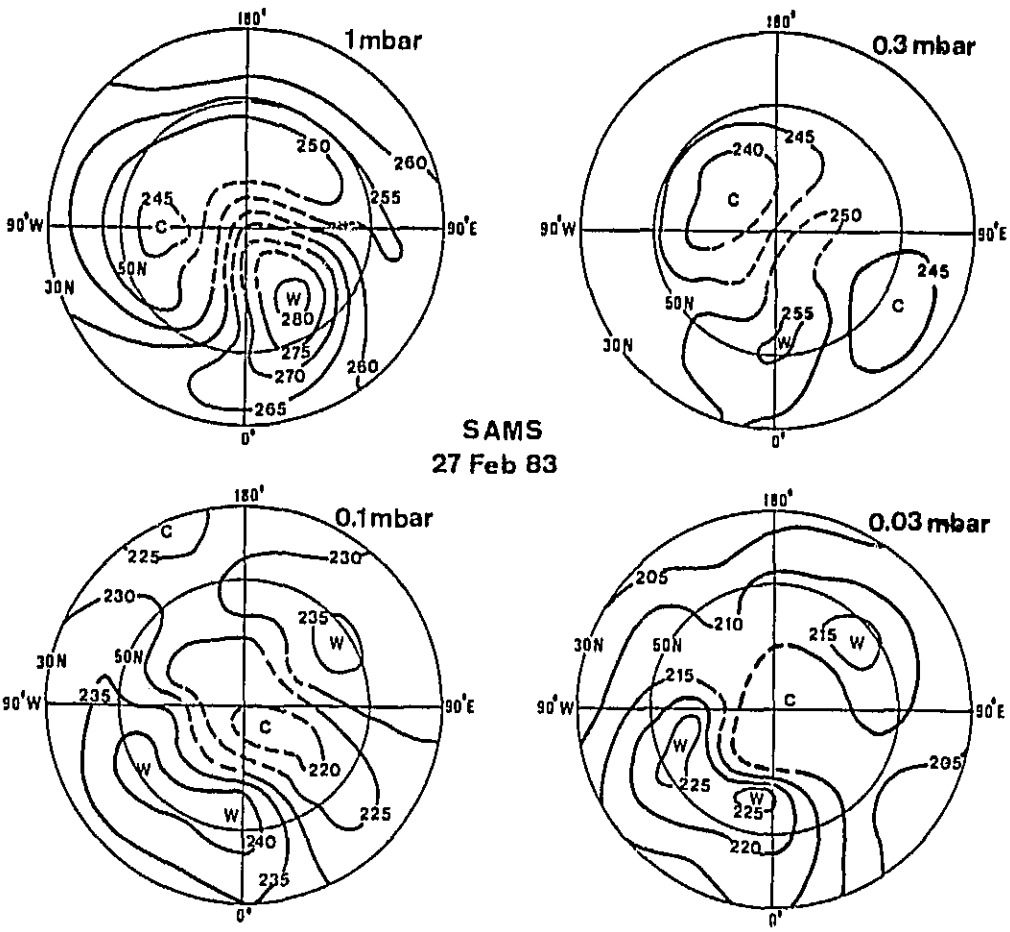

Figure 8. Charts of temperatures [K] retrieved from measurements of the SAMS aboard NIMBUS 7 (courtesy Clarendon Laboratory, University Oxford, UK).

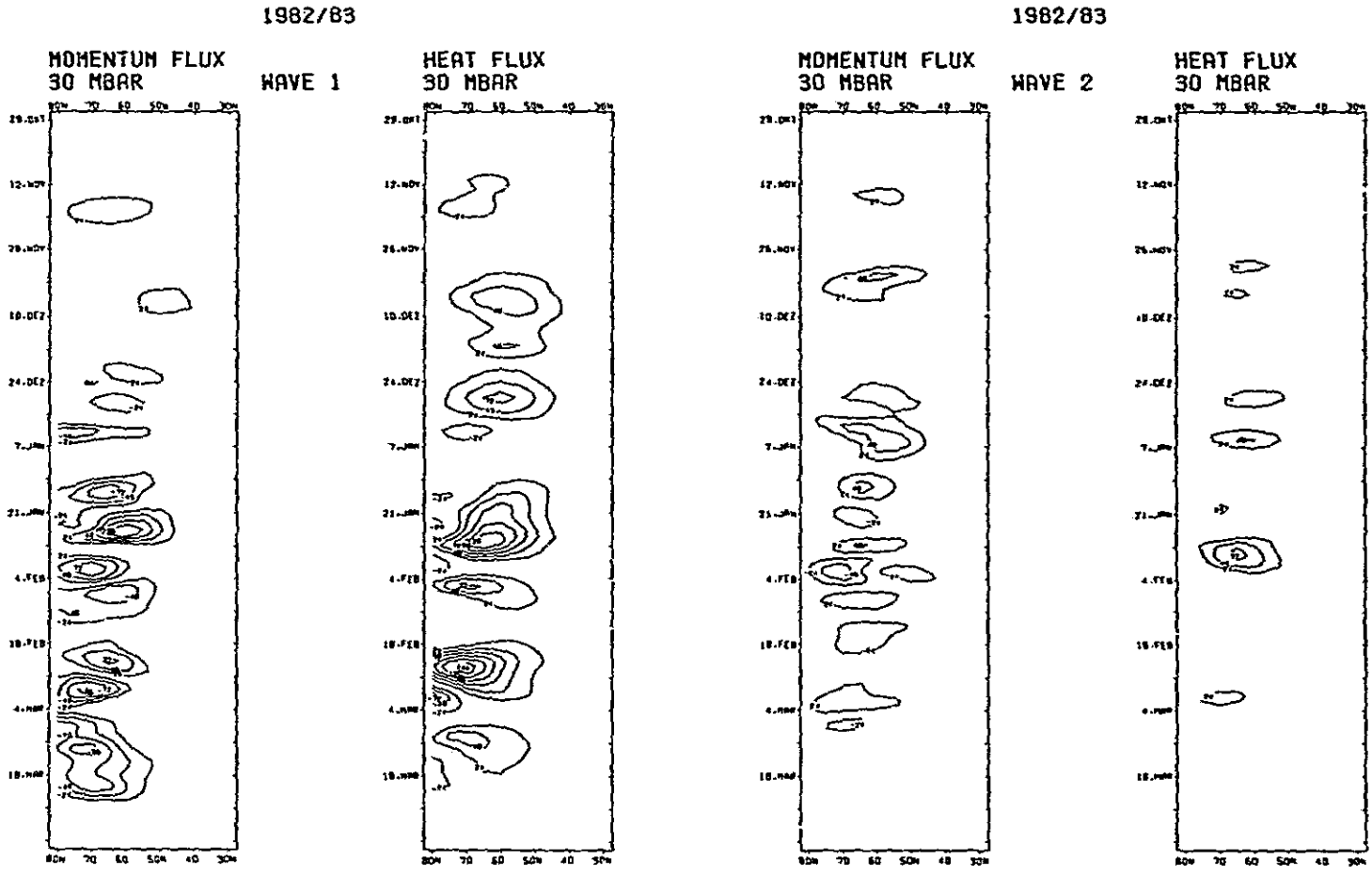

Figure 9. Meridional time sections from November 1982 to March 1983 of zonally averaged eddy momentum transport [$m^2 s^{-2}$] and eddy heat transport [K m s^{-1}] by the planetary waves 1 and 2 at 30 mbar.

CALCULATION OF THE MOMENTUM BUDGET

A transformed momentum equation may show the facts which led to the observed wind changes during this winter. Included in the quasigeostropic form of this equation is the so-called Eliassen-Palm-vector (EP-vector) which shows eddy momentum and sensible heat transport. This vector was introduced because its divergence describes the interaction between the waves and the mean flow (s. Beilage SO 9/82 B). Besides this effect the mean flow can be changed by the mean meridional circulation induced by transient or non steady waves (residual meridional circulation). The balance between this three terms (wind changes with time, divergence of the EP-vector and effect of the mean residual meridional circulation on the mean zonal flow) are plotted with time in Figure 10.

During all three warming pulses (late December, late January, and late February) strong deceleration of the mean zonal wind at 10 mbar (Figure 2a) took place as shown by the negative values of the wind change in Figure 10. It can be seen that during these periods mostly the waves accounted for the deceleration as shown by the convergence (negative values of the divergence) of the EP-flux.

But there are also periods, during which the mean flow was strengthened in spite of the strong decelerating effect of the waves; this happened due to the northward component of the mean meridional circulation. The question arises when can a permanent deceleration of the mean flow in high latitudes be expected, which leads to a breakdown of the polar vortex. Following theoretical arguments a northward directed EP-vector would indicate that wave activity could be focussed into the polar cap. But such a focussing must include a sufficiently deep layer to destroy a vortex reaching up to the lower mesosphere. In Figure 10 those days which were characterized by a northward directed EP-vector at the 10-mbar-level are marked by an 'N'. For 30 mbar the direction of the EP-vector can be taken from Figure 9. As the horizontal component of the EP-vector equals the negative eddy momentum transport, it can be seen, whether for wavenumber 1 or 2 a northward directed EP-flux (i.e. southward directed momentum transport with negative values) occurred in 30 mbar. Though the waves counteracted frequently, the sum of the effect by both waves is similar to the picture of wave 1 because of the much stronger values.

The largest northward transport of wave activity by the EP-flux appeared in the beginning of March, when both waves caused equally directed momentum transport (southward). Accordingly the westerly wind in the polar cap was decelerated, and between 30 and 10 mbar the zeroline of the mean zonal wind, moving successively south- and downward, reached 65°N around 22 March, as can be seen in Figures 2a and 3.

ACKNOWLEDGEMENT

For watching the stratospheric-mesospheric wintertime circulation, preparing the daily STRATALERT messages, and performing this report we got the following additional informations:

- from the Meteorological Office Bracknell, U.K.: Daily charts of radiances for the northern hemisphere at channels 26 and 27 of the SSU (Stratospheric Sounding Unit) onboard of the NOAA satellites and the preliminary 10- and 1-mbar height charts derived from this data;
- from the Claredon Laboratory, University Oxford, U.K.: Retreived temperature distributions over the northern hemisphere at 1, 0.3, 0.1, and 0.03 mbar from the SAMS (Stratospheric and Mesospheric Sounder) onboard of NIMBUS 7;
- from the Geophysical Observatory Collm, GDR: Prevailing winds at mesopause heights over Center Europe from low frequency drift measurements;

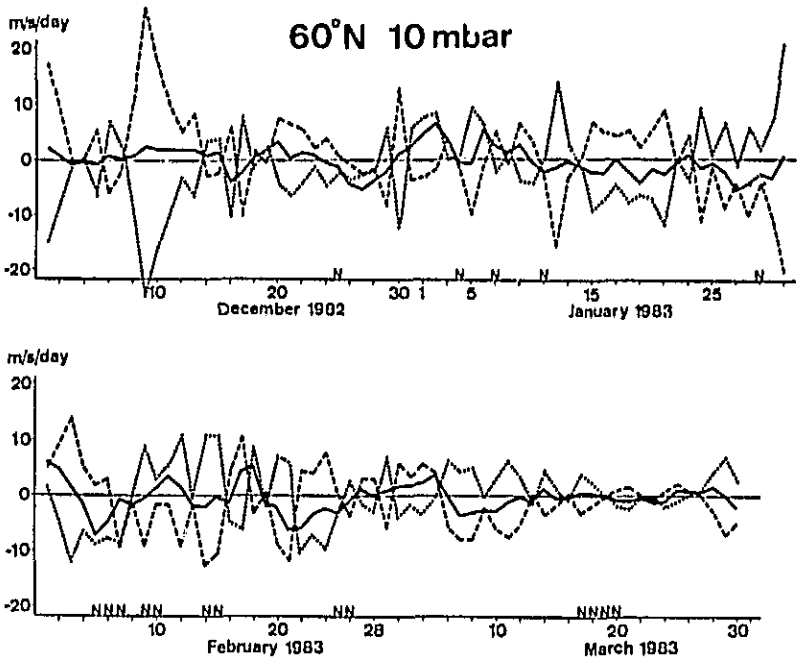

Figure 10. Quasigeostrophic momentum balance at 60°N at 10 mbar
—— Change of the mean zonal wind $\partial\bar{u}/\partial t$ [m s^{-1}/day]
– – – Divergence of the Eliassen-Palm-Vector $\nabla\cdot\mathbb{F}/A\cos\varphi$ [m s^{-1}/day]
····· Coriolis torque $f\bar{v}^*$ of the mean residual meridional circulation
$\mathbb{F}$ and $\bar{v}^*$ as in SO 9/82B, A=radius of the earth, φ=geogr. latitude

- from the Physics Department, University of Saskatchewan, Saskatoon, Canada: Mesospheric winds at three layers over Saskatoon measured with a partial reflection radar;
- from the Department of Physics, University of Sheffield, U.K.: Prevailing winds at mesopause heights over England measured with a meteor radar;
- from the Service d'Aeronomie, Verrieres le Buisson, France: Stratospheric-mesospheric temperature profiles over Haute Provence from lidar measurements;
- from the Norwegian Defence Research Establishment, Kjeller, Norway: Temperatures at 85 km altitude over Kjeller measured with a ground-based infrared spectrometer;
- from the Physical Department, University Wuppertal, FRG: Temperatures at 85 km altitude over Wuppertal measured with a ground-based infrared spectrometer.

All this support is gratefully acknowledged.

For preparing the daily 30- and 10-mbar charts, on which all derived quantities are based, all available radiosonde and rocketsonde observations have been used as well as thickness values derived from satellite soundings (SATEM) for selected orbits. These data are distributed through the Northern hemispheric exchange channels arranged by the WMO.

We thank the members of the Stratospheric Research Group Berlin for the professional and technical assistance.

REFERENCES

Labitzke, K. and B. Grandal (1982), Handbook for MAP, Vol. 5.

Naujokat, B. et al. (1982), Beilage SO 9/82 B.

D2

N85-20447

MAP/GLOBUS CAMPAIGN 1983

D. Offermann

ABSTRACT

The MAP/GLOBUS campaign 1983 is an international campaign of ground-based, airplane and balloon experiments for the study of stratospheric trace constituents. Emphasis is on O_3 and NO_x, and the related solar fluxes and atmospheric dynamics.

This campaign description summarizes the scientific objectives and the experimental set-up as they presently stand. A number of large balloon payloads is to be flown from Aire-sur-l'Adour (France) in September 1983. Their measurements will be co-ordinated with those of an extended network of ground experiments and ozonesonde release stations in Western Europe. A few meteorological rockets will also be launched. The description contains some details of the balloon gondolas, their launch sequence and flight profiles. The campaign time schedule is also given.

SCIENTIFIC OBJECTIVES

The major scientific objectives of the campaign are the accurate measurement of ozone and its short-term variability together with the determination of members of the NO_x-family as NO, NO_2, NO_3, N_2O_5, and HNO_3. Related important solar fluxes (including scattered fluxes) shall be measured as much as possible. Other important trace species (as H_2O) shall be determined simultaneously. The detailed scientific objectives for the ozone measurements are given in Table 1. Table 2 gives respective information for NO_x.

A further scientific objective is the study of atmospheric dynamics, especially of the meteorological background. Therefore special analysis will be performed of the data of respective network stations and satellites. Local wind and turbulence measurements will also be performed.

SURVEY OF THE EXPERIMENTS

(a) Ground-Based Experiments

The ground stations participating in the campaign are listed in Table 3. All stations will measure continuously in September 1983, if not stated differently in Table 3, and if weather allows. To improve the accuracy of total ozone measurements, the Dobson spectrometers should be checked before the campaign.

(b) Balloons and Airplanes

The balloon gondolas to be flown and their experiments are listed in Table 4. Gondola identification numbers, designations and gondola representatives are also given. Major requirements for the flight conditions are listed. They are presented in more detail below. Gondolas G3 and G8 are planned to be flown twice. Experiments of gondolas G2b and G4 are still preliminary.

A grille IR-spectrometer is to be flown on a Caravelle airplane (F. Karcher). The instrument is able to measure column densities of the following species: O_3, N_2O, NO_2, HNO_3, (and also of H_2O, HCl, HF, COS, CO, CH_4). The airplane is available during the first half of September 1983. There are, however, only a few hours of flight time. They shall be used to make an intercomparison measurement with the grille spectrometer on gondola G4.

PRECEDING PAGE BLANK NOT FILMED

Table 1. Scientific objectives: ozone.

1. Improvement of measuring accuracy of ozone instruments by:
   - 1.1 Check of Dobson spectrometers
   - 1.2 Common preparation and handling of Brewer/Mast sondes
   - 1.3 Common calibration of in-situ measuring balloon instruments (before and after the flight)

2. Determination of accuracy of ozone instruments by:
   - 2.1 Comparison of in-situ measurements
   - 2.2 Comparison of remote sensing measurements
   - 2.3 If possible, comparison of remote and in-situ measurements
   - 2.4 Comparison of ground-based and balloon measurements (from one place)

3. Determination of O_3 background field (temporal and spatial structure) by:
   - 3.1 Network of ground stations
   - 3.2 Network of O_3-sonde release stations

4. Reference of balloon O_3 measurements to O_3 background field by:
   - 4.1 Inclusion of (at least) 1 standard Brewer/Mast sonde in all respective balloon gondolas
   - 4.2 Launch of extra Brewer/Mast sondes at all network stations simultaneously with the respective balloon flights (for background use)

5. Time series study of height and absolute value of the maximum in O_3 density by:
   - 5.1 Respective balloon flights (G1 to G5)
   - 5.2 Brewer/Mast sondes (in connection with 5.1)
   - 5.3 Lidars

6. Study of diurnal variation of O_3 at heights above 40 km by:
   - 6.1 High altitude flight of G3

7. Support of determination of atmospheric dynamics by O_3 measurements (both steady state and under possibly disturbed conditions) by:
   - 7.1 Continuous operation of ground station network
   - 7.2 Satellite data
   - 7.3 Regular O_3 sonde release (~3 per week) from network stations, and additional releases on alert

Table 2. Scientific objectives: NO_x

1. Determination of accuracy of NO_x instruments by:
   1.1 Intercomparison of measurements (in situ, remote)
   1.2 Comparison of balloon measurements to airplane and ground-based measurements

2. Study of diurnal variation of NO_x by:
   2.1 Extended measurements during day and night
   2.2 (Nearly) simultaneous measurements of NO, NO_2, NO_3, N_2O_5

3. Determination and interpretation of the NO_2/NO ratio by:
   3.1 Simultaneous measurement of NO and NO_2
   3.2 In addition simultaneous determination of $J(NO_2)$ and O_3

4. Study of the HNO_3/NO_2 ratio by:
   4.1 Simultaneous measurement of HNO_3 and NO_2
   4.2 Selection of undisturbed stratospheric conditions

5. Accurate determination of HNO_3 mixing ratio at altitudes above 30 km by:
   5.1 Comparison of different instruments measuring HNO_3

Table 3. Ground-based experiments.

STATION	EXPERIMENTER	TECHNIQUE/PARAMETER
El Arenosillo 37°N, 7°W	Cisneros	Dobson / O_3
Biscarosse 44°N, 1°W	Lovisa	Dobson / O_3
Aire-sur-l'Adour 44°N, 0°W	Matthews/Flentje	Sol. Abs. / O_3, NO_2
Floirac 45°N, 2°W	Baudry/de LaNoe	Microwave / O_3, CO (During balloon flights: continuous measurements; other days: 11-15 UT approx.).
Uccles 51°N, 4°E	De Muer	Dobson / O_3
Haute Provence 44°N, 6°E	Chanin	Lidar / T, aerosol
	Crochet	ST-radar / T, $\vec{v}$
	Jouve/Marche	IR spectrometer / NO, HCL, HF
		Dobson / O_3
		Umkehr / O_3
	Megie/Pelon	Lidar / O_3
Jungfraujoch 46.5°N, 8°E	Zander	IR spectrometer / HF, HCL, CH_4, CO, NO, N_2O, H_2O, CO_2, O_3 total, HNO_3?
Zugspitze 47.5°N, 11°E	Rothe	Lidar / O_3
Garmisch-P 47.5°N, 11°E	Reiter	Lidar / Aerosol (with co-ordinated radiosonde and ECC sonde flights).
Hohenpeissenberg 48°N, 11°E	Attmannspacher	Dobson / O_3 Brewer / O_3, SO_2 (O_3 Umkehr)
Frascati 42°N, 13°E	Fiocco	Lidar / Aerosol, trace gases (?)

Table 4. Balloon gondolas.

NO/REPRESENTATIVE	EXPERIMENTER	TECHNIQUE	GONDOLA WEIGHT	FLIGHT CONDITIONS
G1/RiO Rippel	Rippel/Offermann	IR spectrometer (emission)	350 kg	40 km float altitude; day/night
	Attmannspacher	Brewer/Mast		
G2a/FaK Matthews/Flentje	Fabian/Flentje	Chemoluminescence (NO, NO_2)		Day flight, valve descent and ascent around noon, float in night, slow descent
	Attmannspacher	O_3: Brewer/Mast		
	Kondo	Chemoluminescence (NO)		
G2b/PoM Pommereau	Pommereau	vis. + UV spectrometer (NO_2, O_3)		2 ascent, 2 descent measurements valve operation near noon
	Murcray	IR spectrometer (absorption)		
	P. Simon	UV photometer/O_3 albedo spectrometer		
	Attmannspacher	Brewer/Mast		
G3/AiM	Matthews/Aimedieu	O_3: chemoluminescence	300 kg (?)	Day flight, valve descent around noon
Matthews/ Aimedieu	Matthews/Aimedieu	Brewer/Mast (3)		
	Cisneros	Decoloration tubes (30)		
	Robbins	Dasibi sonde		
	Krueger	Solar UV abs. (Rocoz)		
	Barat	Anemometer (3D-wind)		
	Perov	Phodamin-B		
	P. Simon	Solar UV-abs.		

Table 4 (continued)

	Attmannspacher	Brewer/Mast		
G4/LouR	Louisnard	Grill Spectrometer	430 kg (?)	40 km float altitude,
Louisnard	Roscoe	PMR (NO, NO_2, N_2O_5)		sunset or sunrise
	Attmannspacher	Brewer/Mast		
G5/Rig	Rigaud	Star occultation (O_3, NO_3, NO_2?)	350 kg	40 km float altitude
Rigaud		Aerosol		night; no moon (6.-17.9.83)
	Attmannspacher	Brewer/Mast		
G6/Arn	Arnold	Ion spectrometer		
Arnold				
G7/ArA	Arijs	Ion spectrometer	340 kg	Valve; slow descent,
Arijs	Ackerman	"CAVENTE"		sunset/sunrise
G8/IIIII	Helten	Matrix isolation	400 kg	day
Helten		Brewer/Mast		valve, slow descent
	Hans/Schurath	N_2O photolysis		
	Harries	Microwave (O_3, H_2O)		
	Junkermann	Solar flux (photometers: 290-315 nm 300-420 nm)		
	Attmannspacher	Brewer/Mast		

(c) Rockets

Twelve Superloki rockets with Data Sondes will be launched from El Arenosillo, Spain (Cisneros, CONIE). They will measure temperatures and winds from 55 km to 20 km. Further meteorological rockets will presumably be launched from Les Landes and/or Brest. Rocket launch scheme is tbd.

(d) Network of Ozonesonde Stations

Ozonesondes (mostly Brewer/Mast sondes) shall be flown from various stations for three purposes:

(1) To establish the O_3 background field by regular launches from all stations every Monday, Wednesday, and Friday during the whole campaign. Launch time is 12:00 UT.

(2) Sondes will be flown on alert together with balloons G1, G2a, G2b, G3, G4, G5, G8 from the stations Huelva, Haute Provence, Hohenpeissenberg, and Uccles. One sonde will be launched from each station, except for balloons G3 and G5: for each of these two balloons there will be 3 Brewer/Mast flights from Haute Provence. It is to be noted that each of the abovementioned balloons carries at least one Brewer/Mast sonde itself. In this way ozone densities during balloon flights can be referred to the O_3 background field.

(3) In the case of peculiar atmospheric events (like passage of a cold front) additional ozonesondes will be released on alert in a coordinated way from the stations mentioned above and from Biscarosse. Launches shall be performed at 6 hourly intervals, starting 2 hours before the event, and continuing until it ends.

The network stations and the number of ozonesondes available are summarized in Table 5. A task group was set up to ensure good accuracy of ozonesonde and ground based ozone measurements. All Brewer/Mast sondes shall be prepared in the same way to guarantee comparability of the data. The task group will meet twice during spring 1983 to discuss related problems (see time schedule below). Members of the group are: Megie, Aimedieu, Cisneros, DeMuer, Hartmannsgruber, Lovisa, Marche, Matthews, Pelon, and Rothe.

Additional ozonesondes (type ECC) are launched at irregular intervals in conjunction with the aerosol lidar measurements at Garmisch-Partenkirchen (R. Reiter).

(e) Radiosonde Network

Routine radiosonde data will be used for stratospheric weather forecasts during the campaign, and for 3D trajectory analysis afterwards. Radiosonde stations available for these purposes are listed in Table 6. Extra radiosondes will be launched from Bordeaux together with the balloons. These are especially intended to improve the temperature determinations. They will be tracked by radar and therefore will have accurate altitude data.

(f) Satellites of Interest for MAP/GLOBUS

Satellites presently in orbit or planned for the near future are listed in Table 7. As concerns SAMS on Nimbus 7, the instrument is collecting data again. Fast evaluation of TOVS data (NOAA6, NOAA7) will be provided by S. Muller (EERM/CNRM, Toulouse) by means of the Lannion station. SME data can be obtained with short time delay through the local data center at Bonn University (Prof. v. Zahn, Physics Department).

Table 5. Ozone sonde network.

STATION	EXPERIMENTERS	TYPE OF SONDE	NUMBER OF LAUNCHES
El Arenosillo 37°N, 7°W	Cisneros	ECC	≤ 30 Mi/We/Fr + 8 on alert
Biscarosse 44°N, 1°W	Lovisa/Karcher	Brewer/Mast	Mo/We/Fr (and 4 on alert)
Aire-sur-l'Adour 44°N, 0°W	Attmannspacher	Brewer/Mast	10 (G1 - G5, G8)
	Aimedieu	Brewer/Mast	3 (on G3)
Uccles 51°N, 4°E	DeMuer	Brewer/Mast	≤ 40 Mo/We/Fr + on alert
Haute Provence 44°N, 6°E	Megie (+Attmannspacher)	Brewer/Mast	30 (+10) Mo/We/Fr + on alert
Cagliari/Elmas 39°N, 9°E		Brewer/Mast	1/week (Wednesday)
Hohenpeissenberg 48°N, 11°E	Attmannspacher	Brewer/Mast	≤ 40 Mo/We/Fr + on alert

Table 6.

	STATION	LATITUDE	LONGITUDE
03 774	Crawley	51.05 N	00.13 W
03 808	Camborne	50.13 N	05.19 W
03 953	Valentia Observatory	51.56 N	10.15 W
06 260	De Bilt	52.06 N	05.11 E
06 447	Uccle	50.48 N	04.21 E
06 476	St.-Hubert	50.02 N	05.24 E
06 610	Payerne	46.49 N	06.57 E
07 145	Paris		
07 110	Brest/Guipavas	48.27 N	04.25 W
07 180	Nancy/Essey	48.41 N	06.13 E
07 480	Lyon/Bron	45.43 N	04.57 E
07 510	Bordeaux/Merignac	44.50 N	00.42 W
07 645	Nimes/Courbessac	43.52 N	04.24 E
07 761	Ajaccio/Campo del Oro	41.55 N	08.48 E
08 001	La Coruna	43.22 N	08.25 W
08 221	Madrid/Barajas	40.27 N	03.35 E
08 579	Lissabon/Port.		
08 302	Palma		
09 548	Meiningen	50.39 N	10.46 E
10 410	Essen	51.24 N	06.58 E
10 739	Stuttgart/Bad Cannstatt	48.50 N	09.12 E
10 866	Munchen/Riem	48.08 N	11.43 E
11 520	Praha - Libus	50.00 N	14.27 E
16 044	Udine/Campoformido	46.02 N	13.11 E
16 080	Milano/Linate	45.26 N	09.17 E
16 242	Roma/Fiumicino	41.48 N	12.14 E
	Ship R	≈47 N	17 W

Table 7.

SATELLITE	INSTRUMENT	PARAMETER
Nimbus 7 until 1985	SBUV TOMS SAMS (?)	Total O_3, radiation Total O_3, radiation T, N_2O, CH_4, H_2O
Tiros N, and NOAA 6, 7	TOVS (HIRS, SSU)	T, total O_3
DMSP (Block 5 D-2 F?)	MFR (?)	Total O_3
SME (3 am, 3 pm)		Solar UV irradiance, T, NO_2, O_3, (H_2O)
FSLP (1 week of Oct. 1983)	P. Simon Girard/Ackerman	Solar flux Grille spectrometer
San Marco 4 (launch autumn 1983)	EUV, UV, vis. spectrometer	O_3 (BUV), NO, sol. flux, albedo
EXOS-C (launch 1984)		CH_4, N_2O, O_3, CO_2, H_2O, aerosol
ERBS (launch June 1984)	SAGE II	Aerosol, NO_2, O_3, H_2O

DESCRIPTION OF BALLOON GONDOLAS

Keyword descriptions of balloon gondolas are given below and sketches of the instrument arrangements are shown in Figures 1 and 2. Gondola 2b is still to be determined. Gondola 4 does not yet show inclusion of the PMR experiment of H. K. Roscoe which is presently planned.

Spectrometer:	Ebert-Fastie, 50 cm focal length
Wavelength:	1-30 μm
Resolution:	2000
Telescope:	Herschel (off axis)
View angle:	Limb scan at float altitude, emission measurement (day, night)
Altitude resolution:	2-3 km
Azimuth:	Controlled by ground command
Coolant:	Liquid helium
NESR:	$2 \cdot 10^{-10}$ W/cm^{2}sr
Calibration:	Black body source and IR lasers
O_3 measuring accuracy:	±30% (estimated)
Weight:	340 kg
Float altitude:	40 km
Altitude range:	10-45 km
Number of flights:	1
Bit rate:	48 Kbits/sec
Commands:	30
Special requirements:	Clean room (mobile unit available), Liquid nitrogen, Liquid helium, Protection against dust during launch preparation

Gondola No. 2a

Table 8 lists the experiments that constitute this payload while Table 9 tabulates the investigators with their institution. See Figure 3 for sketch of Gondola 2a.

Gondola Representative: W. A. Matthews S.A./CNRS
Technical Manager: G. Flentje M P A E

Total Gondola weight (including batteries but excluding CNES telemetry)	240-260 kgs
Approximate dimensions (w x d x h)	140 x 130 x 75 cms
Telecommands	10
Telemetry: Expt 1) PCM 4 channels 5, 7, 11, and 12	
Expt 2) PCM channel 8; 1200 bps	
Expt 3) 1 channel	

Additional payload information. Experiments (1) and (2) exhaust unreacted ozone into the ambient atmosphere. This ozone is generated by silent discharge within each instrument. In experiment (1), a xenon lamp is used to photo-dissociate NO_2 into NO and this additional NO reacts with ozone generated on board. The increased chemiluminescent signal is a measure of the NO_2 in the ambient air. Experiments (1) and (2) are designed to work in the stratosphere since the presence of water vapour lowers the efficiency of the chemiluminescent reaction.

Flight profile. It is planned to fly gondola No. 2a once during the GLOBUS campaign under a 100,000 m^3 balloon with apex valve so that a vertical excursion during the flight and a slow descent at the end of the flight can be made.

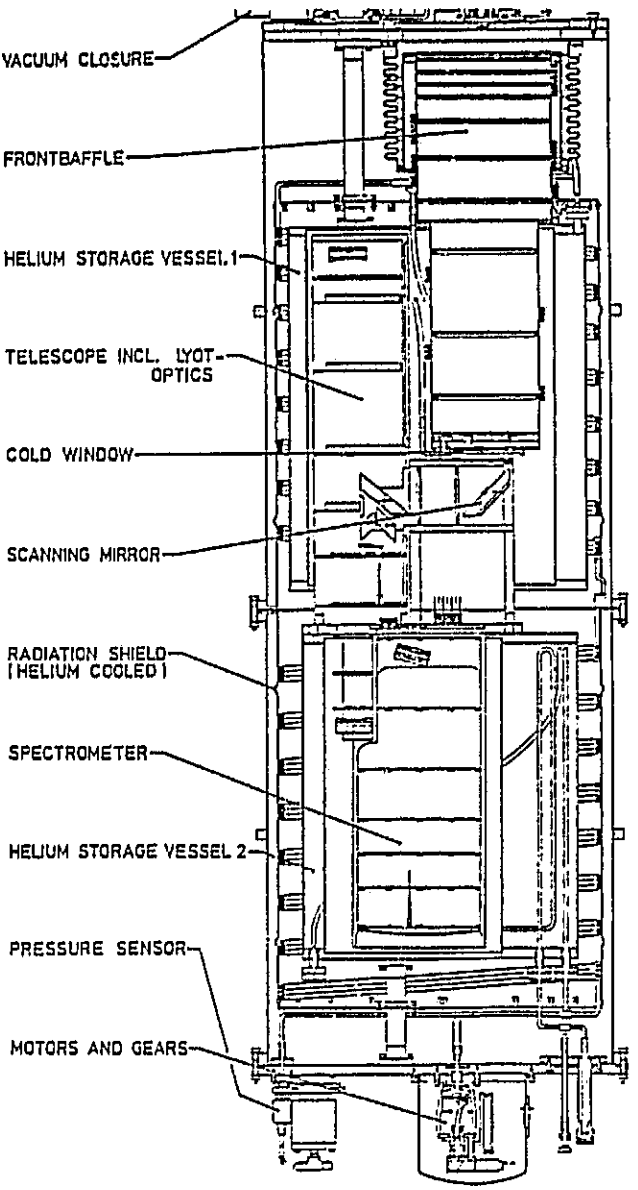
VACUUM CLOSURE
FRONTBAFFLE
HELIUM STORAGE VESSEL 1
TELESCOPE INCL. LYOT-OPTICS
COLD WINDOW
SCANNING MIRROR
RADIATION SHIELD (HELIUM COOLED)
SPECTROMETER
HELIUM STORAGE VESSEL 2
PRESSURE SENSOR
MOTORS AND GEARS

Figure 1.

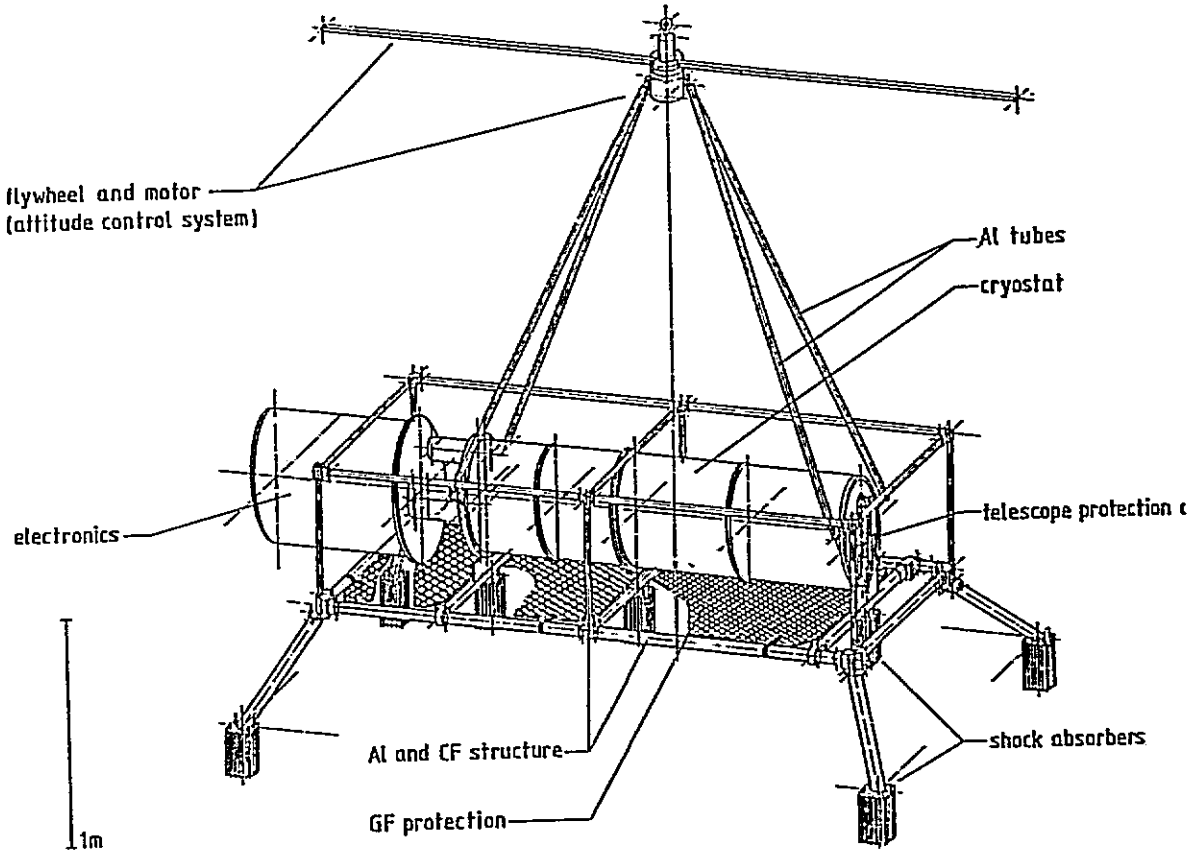
flywheel and motor
(attitude control system)
Al tubes
cryostat
electronics
telescope protection
Al and CF structure
GF protection
shock absorbers
1m

Figure 2.

Table 8.

INSTITUTE	MEASUREMENT PRINCIPLE	PARAMETER	TYPE	RESTRICTION
1) M P A E (Fed. Rep. Germany)	Chemiluminescent (ozone)	NO	in situ	Above 200 mb
	Photodissociation then detection as for NO	NO_2	in situ	" "
2) U of Nagoya (Japan)	Chemiluminescent (ozone)	NO	in situ	" "
3) S.A./CNRS (France)	Brewer/Mast (Wet chemical)	O_3	in situ	First ascent

Table 9.

EXPT N°	INSTITUTION	INVESTIGATORS
(1)	MPAE - Max Planck Institut fur Aeronomie, 3411 Katlenburg Lindau	G. Flentje, P. Fabian, W. A. Matthews
(2)	U.of Nagoya - Research Institute for Atmospherics, Toyokawa, Iichi 442	Y. Kondo
(3)	S.A./CNRS - Service d'Aeronomie, 91370 Verrieres le Buisson	W. A. Matthews P. Aimedieu

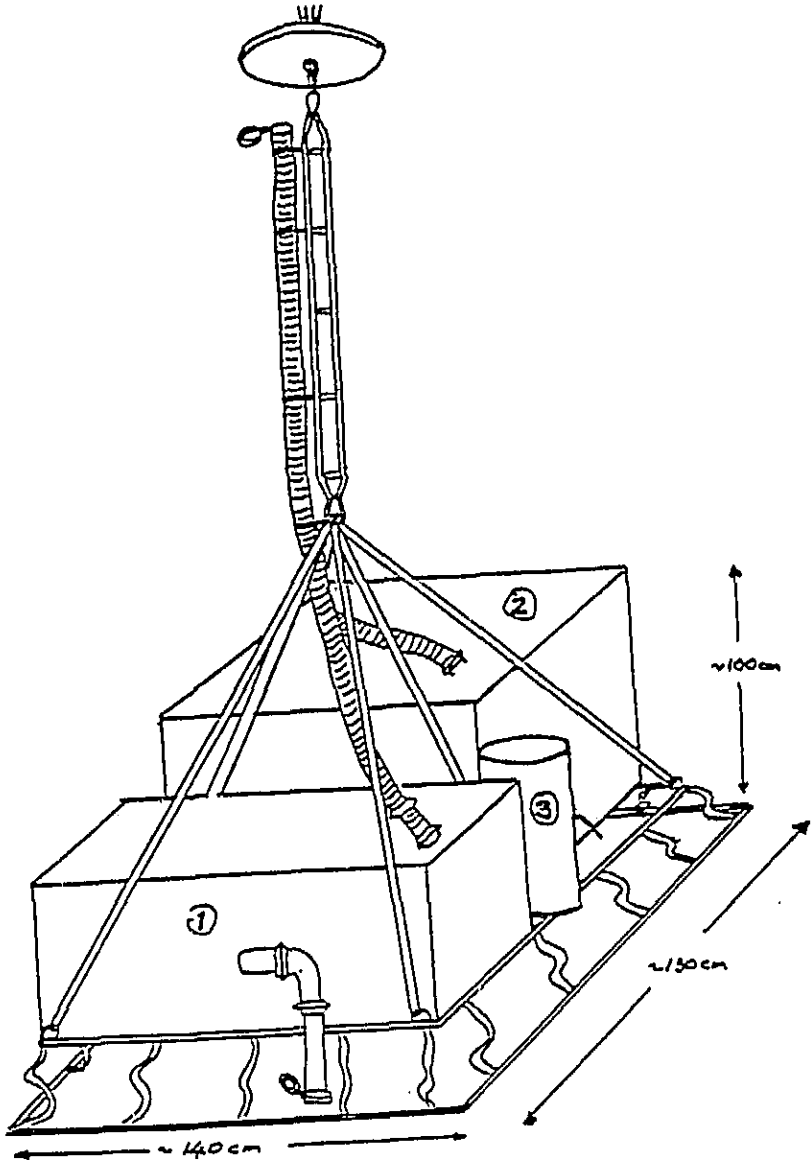

Figure 3.

The proposed flight profile is given in Figure 4.

Gondola No. 3

Table 10 lists the experiments that constitute this payload while Table 11 tabulates the investigators with their institution.

Gondola Representative: W. A. Matthews S.A./CNRS
Technical Manager: C. Malique S.A./CNRS

Total Gondola weight (including batteries but excluding CNES telemetry)	~230 kgs
Approximate Gondola dimensions (w x d x h)	120 x 60 x 320 cms
Telecommands	~27
Telemetry: Expt. 8 has separate 400 MHz 12 bits analog channel and pressure at 30 kHz, 16 bits Expts. 1, 2, 3, 4, 6, 7 multiplexed PCM Expt. 5 - no telemetry	

Additional payload information. Experiment 1 exhausts a reacted olefin.

Experiments 6 and 7 use the sun as their source of radiation for ultraviolet absorption measurements and are fixed at the top of the gondola with diffuser plates on their input windows and are orientated at a fixed elevation angle.

In experiment 5, tubes filled with indigo dye are flushed for 20 minutes sequentially with ambient air and the colour change, measured after recovery, is indicative of the ozone amount that has entered the tube.

With experiment 4, the internal consistency of the Brewer-Mast can be checked.

Proposed flights. It is planned to fly Gondola 3 twice in September from Aire sur l'Adour.

Flight No.1 - 100,000 m^3 balloon with apex valve.
Flight No.2 - 350,000 or 400,000 m^3 (possibly with apex valve).

The proposed flight profiles are given in Figure 5 and instruments in Figure 6.

ONERA Gondola No. 4

(1) Includes the ONERA grille spectrometer (OGRIS) coupled to a sun pointer (infrared absorption spectroscopy) see Figure 7.

(2) The Gondola has a magnetic and sun azimuthal control and is oriented to the sun during sunset and sunrise periods (precision ±1°).

(3) The field of view of the whole experiment is vertically +30° above the horizon; -10° below the horizon; and horizontally ±1°.

(4) The total weight is 350 kg including batteries and telemetry.

(5) Specific features:
Telemetry requirements: PCM telemetry
Bit rate: 8 kbits/sec
The experiment has its own encoder
Commands: 20 discrete
Altitude range 37-42 km. No self measurement of the altitude, the needed precision is ±200 m.

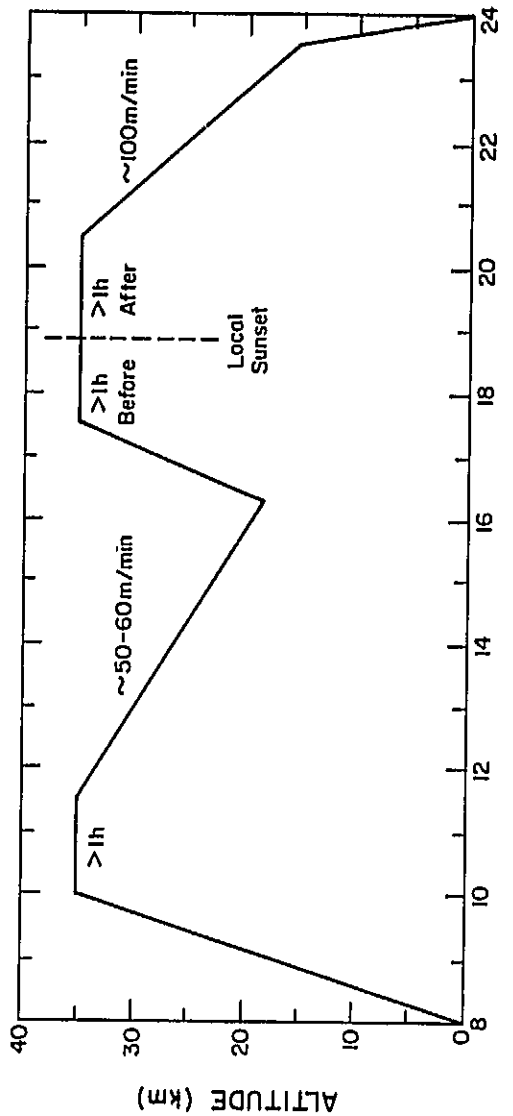
ALTITUDE (km)
0
10
20
30
40
8
10
12
14
16
18
20
22
24
TIME (U.T.)
>1h
~50-60m/min
>1h
Before
Local
Sunset
>1h
After
~100m/min

Figure 4.

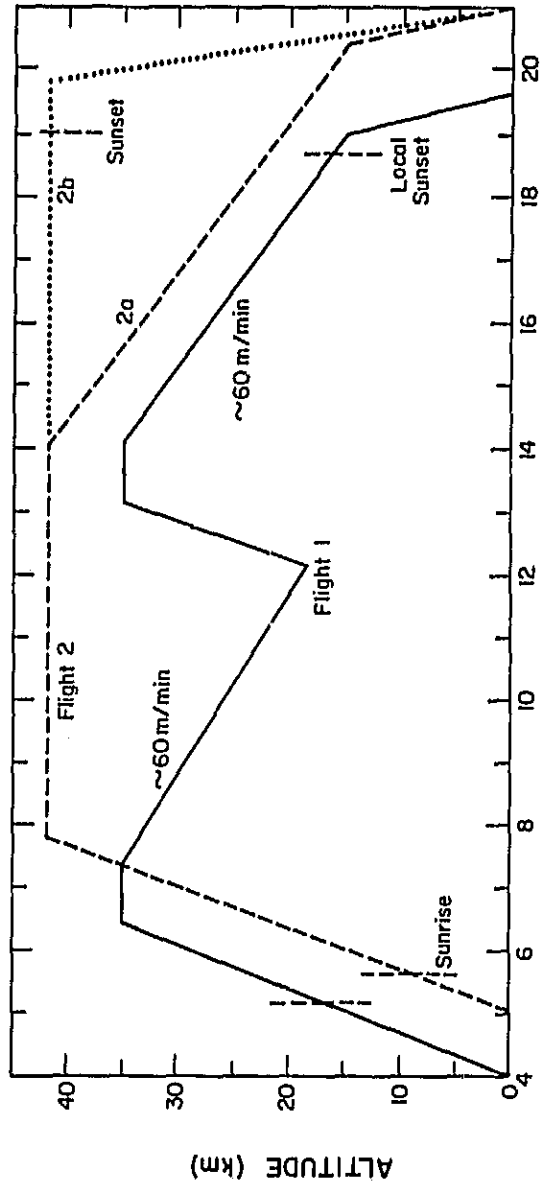
ALTITUDE (km)
0
10
20
30
40
4
6
8
10
12
14
16
18
20
TIME (U.T.)
Sunrise
Local Sunset
Sunset
2b
2a
Flight 2
Flight 1
~60 m/min
~60 m/min

Figure 5.

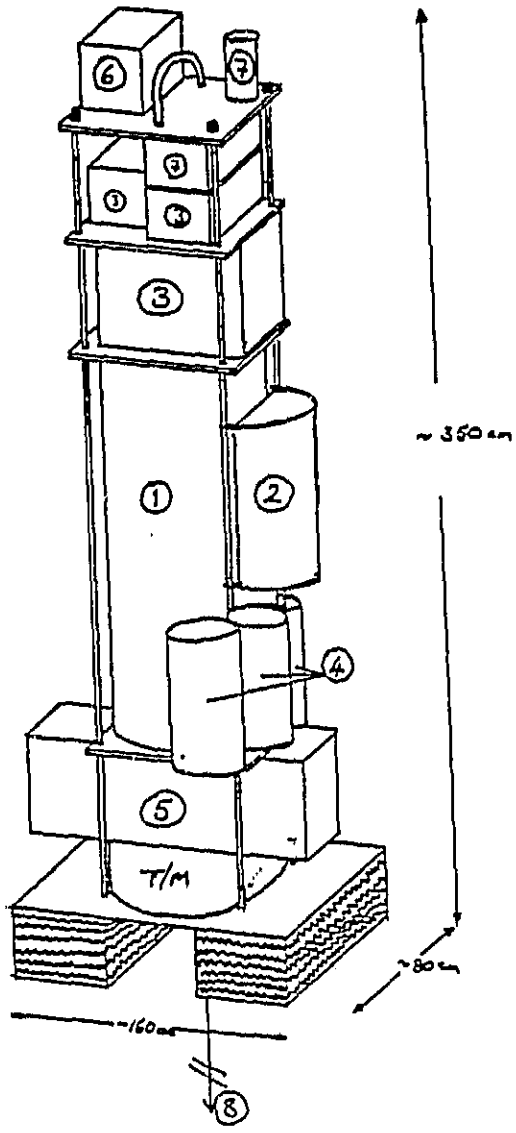

Figure 6.

ONERA GONDOLA 350 KG

Schematic view of the pendular experiment

1. Sun sensor with large field of view
2. Vertical pivot
3. Fine sun sensor
4. Sun-tracker motors
5. Infrared detector
6. Telemetry transmitter
7. Spectrometer (see details below)

All dimensions in millimeters.

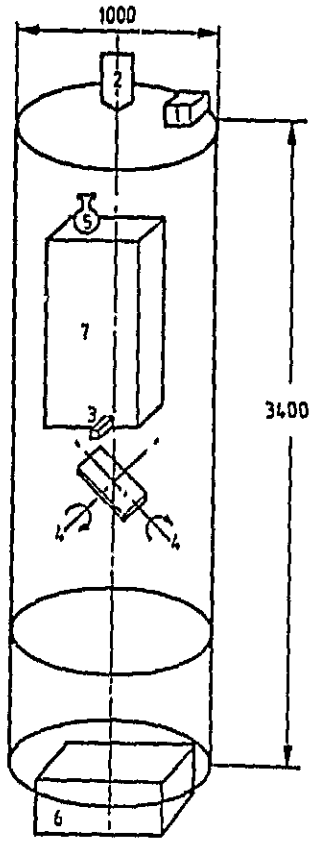

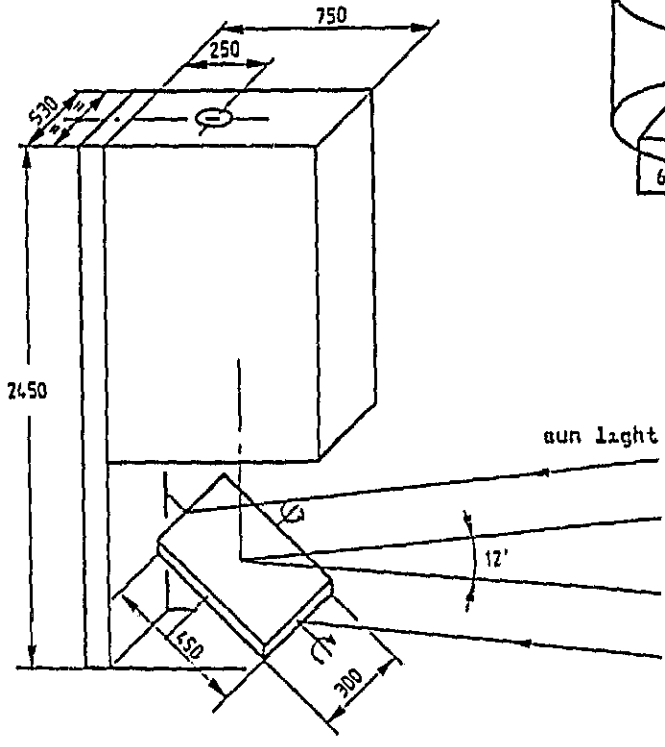

Figure 7.

Table 10.

INSTITUTE	MEASUREMENT PRINCIPLE	PARAMETER MEASURED	TYPE	RESTRICTION
1) SA/CNRS (France)	Chemiluminescent (Olefin)	O_3	in situ	—
2) T.S.A.O. (Russia)	Chemiluminescent (Rhodamine B)	O_3	in situ	—
3) NASA/JFC (USA)	Dasibi type (UV absorption)	O_3	in situ	—
4) SA/CNRS (France)	3 Brewer/Mast (Wet Chemical)	O_3	in situ	First ascent
5) CONIE (Spain)	Decolouration tubes (indigo blue)	O_3	in situ	20 min sampling
6) IASB (Belgium)	Filter photometer (UV absorption)	O_3	Remote	Sunlight
7) NASA/GSFC (USA)	Filter photometer (UV absorption)	O_3	Remote	Sunlight
8) SA/CNRS (France)	Ion - anemometer	3 D wind vector	in situ	—

Table 11.

EXPT. N°	INSTITUTION	INVESTIGATORS
1 & 4	S.A./CNRS - Service d'Aeronomie 91 370 Verrieres le Buisson	W. A. Matthews & P. Aimedieu
2)	T S A O - Hydrometeorological & Environmental Central Observatory, Moscow	S. P. Perov
3)	NASA/JFC - Johnson Flight Center, Houston, TX 77058	D. Robbins
5)	CONIE - INTA, Madrid	J. M. Cisneros
6)	IASB - Institut d'Aeronomie Spatiale de Belgique, Bruxelles	P. Simon
7)	NASA/GSFC - Goddard Space Flight Center, Greenbelt, MD 20771	A. Krueger
8)	S.A./CNRS - Service d'Aeronomie, 91370 Verrieres le Buisson	J. Barat & P. Aimedieu

Cryogenic coolant: liquid nitrogen
Environment perturbations: very sensitive to vibrations and electric fields.

(6) Measured species and precision. The error bars are indicated at 30 km.
O_3 (±0.5 ppm) H_2O (±1 ppm)
CH_4 (±0.05 ppm) N_2O (±20 ppb)
NO (±1 ppb) NO_2 (±0.25 ppb) HNO (±1 ppb)
HCl (±0.2 ppb)
CO (±1 ppb) COS (±0.1 ppb at 20 km)
The vertical resolution is 0.5 km at 40 km and 2 km at 20 km.
Spectra are obtained from 1300 to 3000 cm^{-1} with a spectral resolution of 0.1 cm^{-1}.

Description of the Gondola 5

(1) Parameter to be measured: O_3, NO_3, Aerosol

(2) Measurement technique: Occultation of stars by the earth's atmosphere, observed from an altitude of up to 40 km.

(3) Outline description of the instrument: We are using the stellar balloon package of the Observatory of Geneva with its pointer based on an image-dissector tube. Light is collected by an F 5 Cassegrain telescope, with an aperture of 200 mm diameter. The mirror substrates are of "Zerodur" glass and the mountings are of invar; by these means focus is ensured between +30 and -40°C. Spectral analysis is done with a double-pass monochromator, type Jobin-Yvon DH 10. The detector is a photomultiplier, with a trialkali cathode, operated in the photon counting mode. The instrument covers the spectral range 200-800 nm. The optical resolution of the spectrophotometer is 0.1 nm. In practice the resolution is limited to 0.6 nm by the precision of the star-tracker, which is 20 arc seconds. In this experiment, a spectral span of 25 nm (647-672 nm) is swept cyclically in 0.2 nm increments in 6.4 s with a final resolution of 1 nm

(4) Altitude region of measurement: 15-40 km.

(5) Altitude resolution: Better than 0.5 km.

(6) Experimental limitations: Measurements only at night, no moon.

(7) Weight: 350 kg including star-pointed nacelle.

(8) View direction of experiments: East with the rising planet Venus.

(9) Draft agenda for campaign MAP/GLOBUS 1983 with the rising planet Venus:

DATE	BEGINNING OF THE CEILING
6 September	2 h 30 GMT
10 September	2 h 10 GMT
14 September	1 h 50 GMT
18 September	1 h 30 GMT

Gondola 7 - Ion-CAVENTE Gondola (Brussels)

(1) Experiments included: Ion mass spectrometer; and CAVENTE - detection of aerosols by photographic techniques.

(2) View direction: Sun pointer (±1° azimuth) (only necessary for CAVENTE).

(3) Field of view: 36° x 36°

(4) Gondola weight: 340 kg including CNES TM + TM package (about 18 kg).

(5) Telemetry and telecommand: Standard CNES analog telemetry with 9 IRIG channels is used. Remote control is by bistable relays in the CNES package (2 different addresses).

(6) Additional measurements: Temperature - bead thermistors; Pressure - (high precision baratron).

(7) Cryogenic coolants needed: Liquid helium for cryopump of ION-payload.

(8) Remarks: Both experiments are working independently from one another and have their own power supplies included. Weight of each can be kept at about 150 kg (including shock absorber) when launched separately. Two identical ion mass spectrometers are available and can be launched together. If necessary one ion mass spectrometer can be combined with another instrument to form a new payload. The second instrument however should be a non-polluting payload, in view of the high sensitivity of the ion mass spectrometer for contaminant gases.

Gondola 8 (HHH)

(1) Participants: Dr. M. Helten, Kernforschungsanlage Julich GmbH, Inst. fur Atmospharische Chemie, FRG; W. Hans, Univ. Bonn, Institut fur Phys. Chemie (Prof. Dr. U. Schurath) FRG; and Dr. Ch. Gibbins, Rutherford Appleton Lab. (RAL), U.K.

(2) Weight: 420 kg

(3) Experiments: (a) Cryosampler IV (KFA), in situ sampling of 10 radical samples (HO_2, NO_2) in different altitudes; (b) Photolysis of N_2O (Univ. Bonn); (c) Radiometers for measurements of O_3 and H_2O (RAL); (d) Mastsonde for O_3 (Dr. Attmannspacher, FRG); (e) Mastsonde for O_3 (KFA); (f) Air temperature by VIZ-Thermistor, 0, 1°C resolution; (g) Air pressure by Paroscientific-Transducer, 0.01 mbar resolution; (h) Photonflux 290-315 nm and 300-420 nm by 2 filter radimeters (KFA; Dr. Junkermann).

(4) Telemetry: PCM- and digital TC-Systems of CNES for 1), 5), 6), and 7) FM-System of CNES for 2) and 4); Special PCM-System of RAL on CNES subcarrier and TC by relais of CNES for 3).

BALLOON LAUNCH SEQUENCE AND FLIGHT PROFILES

Considering the scientific objectives as well as technical and logistical constraints, the following flight sequence was set up;

day 1	Gondola	G3	(AiM)
day 2	Gondola	G8	(HHH)
2	Gondola	G2a	(FaK)
day 5	Gondola	G1	(RiO)
5 + 6	Gondola	G5	(Rig)
6	Gondola	G4	(LouR)
day 7	Gondola	G2b	(PoM)

day 10	Gondola	G8	(HHH, second flight)
10	Gondola	G7	(ArA)
day 11	Gondola	G3	(AiM, second flight)
day 12	Gondola	G6	(Arn)

Immediately before day 1 CNES will perform a technical flight (day 0) to check on turn around conditions. The gaps between days 2 and 5, and days 6 and 9, respectively, are due to logistic reasons. CNES will try to shorten the gap between days 2 and 5, if possible, i.e., if recovery conditions are favourable. Flight G2b (day 5) and the second flight of G3 (day 10) definitely need radar tracking, i.e., cannot be performed during week-ends.

The details of the flight scheme (flight profiles) are as follows:

DAY	TIME (UT)		EVENT
1	04:30	G3	launch
	07:00	G3	at float altitude (35 km)
	08:00	G3	starts slow descent (to 18 km)
	12:30	G3	starts second ascent
	14:30	G3	at float altitude
	15:30	G3	starts slow descent (to 18 km)
	19:30	G3	starts final descent
	20:30	G3	on ground
2	06:30	G8	launch
	08:30	G8	at float altitude (35 km)
	09:30	G2a	launch
	10:30	G8	starts slow descent (to 18 km)
	12:00	G2a	at float altitude (35 km)
	13:00	G2a	starts slow descent (to 18 km)
	15:00	G8	starts final descent
	15:45	G8	on ground
	16:00	G2a	starts second ascent
	17:30	G2a	at float altitude
	19:30	G2a	starts slow descent (to 15 km)
	23:00	G2a	starts final descent
	24:00	G2a	on ground
5	13:00	G1	launch
	16:00	G1	at float altitude (40 km)
	21:30	G1	starts descent
	22:30	G1	on ground
	22:30	G5	launch
6	01:30	G5	at float altitude (40 km)
	01:30	G4	launch
	04:30	G4	at float altitude (40 km)
	05:00	G5	starts descent
	06:00	G5	on ground
	11:00	G4	starts descent
	12:00	G4	on ground
7	05:30	G2b	launch
	07:30	G2b	at float altitude (35 km)
	12:00	G2b	starts slow descent (to 20 km)
	16:30	G2b	starts second ascent
	18:30	G2b	at float altitude

	19:00	G2b	starts descent
	20:00	G2b	on ground
10	06:30	G8	launch (2. flight)
	09:00	G8	at float altitude (35 km)
	11:00	G8	starts slow descent (to 15 km)
	14:45	G7	launch
	16:00	G8	starts final descent
	16:45	G8	on ground
	17:00	G7	at float altitude
	19:00	G7	starts slow descent (to 15 km)
11	00:00	G7	starts final descent
	00:45	G7	on ground
	05:00	G3	launch (2. flight)
	08:00	G3	at float altitude (> 40 km)
	18:30	G3	starts descent
	19:30	G3	on ground
12		G6	

TIME SCHEDULE

Turn around at Aire-sur-l'Adour is expected between 5th-10th of September. The MAP/GLOBUS 1983 campaign will have 2 weeks of priority at the Aire-sur-l'Adour launch facility, starting with turn around. The time table given below was planned accordingly.

Apr. 25-27, 1983	Ozone task group meets at Munich (preparation of data handling/processing).
May 16-21, 1983	Ozone task group technical meeting at Hohenpeissenberg (common procedure for Brewer/Mast sonde preparation).
June 1983	Standard temperature sensor test flight.
Middle of June 1983	Meeting of gondola representatives at Gap (if necessary).
Summer 1983	Dobson spectrometer intercalibration.
Aug. 15, 1983	Arrival of experiments at Aire-sur-l'Adour, earliest possible access to the range for gondola preparations.
Aug. 22, 1983	Begin telemetry tests.
Sept. 1, 1983	Begin campaign, start of ground-based measurements and Brewer/Mast sonde releases.
Sept. 5, 1983	Gondolas G1, G2a, G3, G4, G5, G8 ready for launch; arrival of G7 (Sept. 8, 1983: G7 ready for TM integration); and telemetry integration of G2b to take place on days 3 and 4.
September 1983	Meeting on data formats (at Aire-sur-l'Adour).
Sept. 30, 1983	End of ground-based and Brewer/Mast measurements.

Jan. 23-27, 1984	First post flight meeting (at GSF, Munich), formation of working groups for preparation of integrated papers.
June/July 1984	Second post flight meeting (at Graz, during COSPAR meeting 25.6-7.7.84); preparation of integrated papers; and presentation of single experiment results at COSPAR.
1. week September 1984	Third post flight meeting (at Tessaloniki, during IOC Quadrennial Ozone Symposium), preparation of integrated papers for joint publication, respective presentations at the symposium.

MAP/GLOBUS STEERING COMMITTEE

M. Ackerman	BISA, Brussels
M. Auger	CNES, Paris
H. Bauer	GSF, Munchen
G. Brasseur	BISA, Brussels
M. L. Chanin	CNRS, Verrieres-le-Buisson
P. Crutzen	MPI, Mainz
G. Fiocco	CNR, Roma
J. Harries	RAL, Chilton
T. Itoh	ISAS, Tokyo
A. Kuminov	St. C. Hydromet, Moscow
N. Louisnard	ONERA, Chatillon
D. Murcray	University of Denver
D. Offermann	University of Wuppertal
U. Schmidt	KFA, Julich
R. Watson	NASA, Washington

N85-20448

REPORT ON THE WORKSHOP ON INTERCOMPARISON OF SOLAR U.V. IRRADIANCE MEASUREMENTS AND RELATED INSTRUMENT CALIBRATION

P. C. Simon

The knowledge of the absolute value of the solar ultraviolet irradiance did not improve very much during the rising phase of the solar cycle 21. The variations associated with the solar rotation period have been observed by means of three satellites namely, the Atmospheric Explorer E (AE-E), Nimbus 7 and the Solar Mesospheric Explorer (SME). They led to quantitative values which have been discussed previously. Long-term variations related to the solar activity cycle are not well known. Values were deduced during the solar cycle 21 from the AE-E satellite and the rocket program performed by the Laboratory for Atmospheric and Space Physics (LASP) leading to variations of about a factor of 2 around 150 nm but definitely less than 20 percent beyond 175 nm. Such low level of variation is still masked by the current uncertainties and reproducibility of the observations performed since 1976.

The uncertainties of recent observations are reported in Table 1 with their discrepancies. The gaps between the current accuracy goals and the achievements are still very important. The challenge for the next three years is to improve both the accuracy and the precision of future observations at the level of the available irradiance standards and to measure quantitatively long-term variations of the order of a few percent. The main causes of these gaps have been clearly identified. They are induced by:

1. The diversity of the calibration techniques and standards used for the various solar spectrometers.

2. The calibration accuracy transfer.

3. The lack of intercomparison of standards.

4. The lack of interaction between standards-builders and standards-users.

5. The degradation of the instrument sensitivity due to the contamination of materials.

6. The lack of intercomparison of solar spectrometer responses.

All these problems can and should be solved before the space shuttle program for solar irradiance monitoring starting in 1986 and the launches of the Upper Atmosphere Research Satellites (UARS) scheduled for the end of the 1980's.

The available calibration procedure and performance have been intensively discussed. It turns out that the most accurate spectral irradiance transfer source standards are the Synchrotron Users Radiation Facility (SURF) and the Tungsten Halogen lamp, both being developed at the National Bureau of Standards. The spectral range covered by the tungsten source is limited to wavelengths greater than 250 nm. In both cases, the accuracy in the ultraviolet range is better than ±3 percent. The uncertainties of the SURF have been recently reduced to ±1.3 percent. Its stability is claimed to be better than 1 percent. The main problem occuring in the calibration of solar spectrometers by using this latter standard source is the polarization of the output beam. On the other hand, the uniformity of the beam has been disputed.

Portable sources like the Argon mini-arc and the deuterium lamp are easier to handle than the SURF but their uncertainties are not lower than ±5 percent.

PRECEDING PAGE BLANK NOT FILMED

Table 1. Uncertainties on solar ultraviolet irradiance measurements and future needs.

		Wavelength intervals (nm)					
		Ly-α	135-175	175-210	210-240	240-400	330-400
Accuracy		± 30%	± 30-20%	± 30-20%	± 20-10%	± 10-4%	± 4-2%
		± 10%+	± 10%+	± 10+			
Achieved accuracy on irradiance values		± 30%	± 30%	± 20%	± 15%	± 10%	± 3%
Discrepancies		200%	100%	40%	20%	20%	8%
Uncertainties on spectral irradiance transfer source standards			± 10%	± 6%	± 5%	± 3%	± 2%
		± 3%*	± 3%*	± 3%*	± 3%*	± 3%*	± 3%*
27-d variability		100-30%	12%	10-4%	2%	2-1%	
11-yr variability		100%	< 120%	< 20%	< 10%§	< 5%§	< 2%§
Goals	accuracy	± 10%	± 5%	± 5%	± 5%	± 5-2%	± 2%
	precision	± 5%	± 5%	± 2%	± 1%	< 1%	< 0.1%

+ at 2σ level, using the SURF as calibration standard

* Synchrotron Users Radiation Facility (SURF), at 2σ level

§ according to model calculations published by LEAN ET AL. (1982).

New absolute detectors, namely the silicon photodiodes are presently studied for ultraviolet radiometric purposes at the NBS and are very promising with uncertainties less than 1 percent.

The intercomparison between the various source standards has been initiated by several laboratories and the first results presented during this workshop showed a difference of the order of 20 percent between the deuterium lamp and the SURF, using the Solar Ultraviolet Spectral Irradiance Monitor (SUSIM) experiment developed by the Naval Research Laboratory (NRL) for Spacelab 2. The intercomparison of deuterium lamps calibrated at the NBS and the NPL gives an agreement within a few percent for the relative scale but the absolute calibration can vary from 1 to 16 percent for different lamps. This work has to be completed in order to understand the causes of such divergences between calibration results performed by two different laboratories.

In conclusion, the goals in solar ultraviolet irradiance measurements could be reached in the near future only if the following requirements are fulfilled:

(a) Requirements on the Intercomparison of Spectral Irradiance Standards

Three standards are currently used to define the absolute radiometric reference scale: (1) the synchrotron; (2) the hydrogen arc; and (3) the blackbody.

Practically, the Argon mini arc and the Tungsten Halogen lamp are referred respectively to the hydrogen arc and to the blackbody. Therefore, it is recommended to calibrate the same solar spectrometers against the three different radiometric scales in order to see which source is the best suited to become the prime standard in the future. Direct comparison of the SURF with the blackbody and with the Hydrogen arc needed for that purpose.

The intercomparison of the available standards should continue in order to measure the error sources related to the absolute calibration and the reproducibility of the ground facilities, and to the calibration accuracy transfer. For that purpose, laboratory spectrometers can be used but current and future solar spectrometers should also be utilized in order to detect the errors specifically introduced by each observing instrument. Scientists involved in both radiometry and solar irradiance measurements should work together in the calibration program in order to reduce the errors introduced during the radiometric scale transfer procedure.

(b) Requirements on the Intercomparison of Solar Spectrometers

All solar instruments used by different groups should be cross-calibrated in order to make possible the intercomparison of the data obtained at different epochs. This is particularly true for rocket- and balloon-borne solar spectrometers used for long term variation studies and for measurements of sensitivity drift of free-flyer instruments over large periods of times. Up to now, the SURF seems the most appropriate standard source in the ultraviolet because of its high level of reproducibility and of accuracy and its wide wavelength range. Nevertheless the other transfer standards should be improved further and each group should maintain their own calibration methods by measures of conservation. It should be pointed out that the calibration procedure against the SURF is an experiment by itself requiring time to be scheduled in the future observing program. Comparisons between various solar spectrometers should also be made using the sun as a common source. Measurements should be performed from the same platform. For intercomparisons at wavelengths beyond 190 nm, large stratospheric balloons can be easily used. Such an intercomparison program could be scheduled for 1984. As this kind of flight deals with comparison of in situ solar irradiance measurements in the same environmental conditions, at the

same time and altitude, the uncertainties related to the residual stratospheric absorption corrections applied in order to obtain extraterrestrial fluxes are not introduced when comparing the data.

In the near future, intercomparison on board the space shuttle could be performed in order to cover the full vacuum ultraviolet range. It could also be used to check the instrument behavior in a flight environment comparable to rocket and satellite observations. Studies on instrument degradation could also be made by recovering the instrument after several weeks in orbit.

(c) Requirements on the Satellite Measurements

The errors introduced by the measurement in the space environment should be reduced by appropriate techniques minimizing the causes of degradation of the instrument sensitivity and by controlling their consequences. Future satellite instruments devoted to solar irradiance measurements should satisfy several design requirements in order to minimize the number of optical elements and the number of potentially outgassing surfaces and elements. In particular this can be achieved by completely isolating the electronics from the optics, using tight containers and encapsulated wires and harnesses. The existence of a cold trap on the spacecraft should also reduce the degradation due to outgassing. The assembly, integration and calibration phases should be made using the highest class cleanliness facilities. The solar observations should start several weeks after lift-off to complete the outgassing. Flyable calibration sources should be developed and tested for instance on board the space shuttle, to be available as soon as possible for future missions.

(d) Requirements on the Validation of Satellite Data

In order to validate the satellite data, the instrument aging should be measured by monitoring its radiometric characteristics using flyable calibration standards and techniques. Periodic accurate observations by means of balloon-, rocket- and space shuttle-borne instruments should be performed in order to obtain frequent re-calibration of the satellite solar spectrometer. Balloon measurements have the advantage of no outgassing problem and no damage due to solar ultraviolet or X-ray radiation. Post-flight calibrations are possible. These observations are limited in wavelength and data around 210 nm at 40 km need corrections due to the residual stratospheric absorption. Therefore, the achievable accuracy is of the order of 6 to 7 percent in the stratospheric optical window. Beyond 290 nm, the balloon observations can be performed with an uncertainty limited by the accuracy of the available standards (less than 2 percent) and of the calibration transfer. Reproducibility of 1 percent is now achievable and does permit one to distinguish between any free-flyer instrumental drift and true solar variations at the same level of precision. Ground measurements beyond 330 nm need atmospheric correction which reduce the final accuracy and precision of the data. Rocket measurements cover all wavelengths but the flight environment is rather harsh. The short flight duration does not allow in-flight calibration. Post-flight calibrations are also possible. Uncertainties less than 5 percent are now achievable below 200 nm by using adequate calibration standards and transfer procedures like the SURF.

In the near future, the space shuttle will provide an additional platform for calibration purposes. In addition, instrument retrieval by shuttle flights may help to study the reasons for instrument degradation and would permit post-flight calibration of a satellite solar spectrometer.

ACKNOWLEDGEMENTS

We are grateful to Drs. N. Sundararaman and J. Rogers and to Mrs. Flo Ormond for their hospitality at the Federal Aviation Administration and their help during the workshop.

ANNEX

Resolution adopted by the International Association of Meteorology and Atmospheric Physics (IAMAP) at the III IAMAP Scientific Assembly, Hamburg (FRG), 1981.

considering that solar ultraviolet irradiance (i.e., 100-400 nm) and its temporal variations are not sufficiently well known for middle atmospheric science and that new observations are badly needed to improve the accuracy and the precision of irradiance values, and

recognizing that improvements in calibration procedure are expected to close the gaps between current accuracy goals and achievements,

recommends the improvement of calibration of new instrumentation by means of (a) maintenance of synchrotron calibration facilities, (b) intercomparison of the different spectral irradiance standards, and (c) study of the feasibility of establishing a reference to insure the highest possible precision and intercomparability of future observations.

WORKSHOP ON INTERCOMPARISON OF SOLAR UV IRRADIANCE MEASUREMENTS AND RELATED INSTRUMENT CALIBRATION

May 11 and 12, 1982
Washington, D.C.

PROGRAM

Tuesday, May 11

A. Solar cycle 21 observations

Current knowledge of solar irradiance values related to middle atmosphere processes		P. C. Simon
Variability of solar UV irradiance		G. E. Brueckner
New results:	SME/Rocket	G. J. Rottman
	SBUV	G. F. Heath
	Balloon/Rocket	J. E. Mentall
	Lyman-alpha measurements	J. P. Delaboudiniere

B. UV spectral irradiance transfer standards

SURF II	R. P. Madden
ORSAY synchrotron	J. P. Delaboudiniere
Arc sources	W. R. Ott
D2 lamps	P. J. Key
VUV window diode	R. P. Madden
Silicon photodiode	J. Geist
Tungsten Halogen sources	H. Kostkowski

C. Results on intercomparison of spectral irradiance standards

PTB-NBS intercomparisons	R. P. Madden
NPL-NBS intercomparisons	W. R. Ott
D2 lamps - SURF intercomparisons	J. W. Cook

Wednesday, May 12

D. Calibration of available and future instruments for solar UV irradiance observations

Balloon and rocket		J. E. Mentall G. J. Rottman P. C. Simon
Space Shuttle	SUSIM	M. E. Van Hoosier
	STAS	W. H. Parkinson
	Solar spectrum	P. C. Simon

Satellites	NOAA	W. K. Fowler
	SME	G. J. Rottman
	UARS	G. J. Rottman
		M. E. Van Hoosier

E. Definition of future intercomparison strategy

Group discussion on:

- intercomparison of portable standards
- intercomparison of non-portable standards
- intercomparison of instruments
- transfer of radiometric scale on instruments

PARTICIPANTS

P. C. Simon, Convenor
J. Bartoe
J. Bridges
G. Brueckner
S. Chandra
J. Cook
J. Delaboudiniere
W. Fowler
J. Geist
D. Heath
E. Hilsenrath
H. Kostkowski
R. Madden
J. Mentall
W. Ott
H. Park
W. Parkinson
E. Reeves
J. Roger
G. Rottman
P. Smith
H. Van Hoosier
D. Williams
R. Watson

N85-20449

MSG-7: MOLECULAR ABSORPTION PROCESSES RELATED TO THE PENETRATION OF ULTRAVIOLET SOLAR RADIATION INTO THE MIDDLE ATMOSPHERE

J. E. Frederick (Chairman)

Members: A. J. Blake, D. E. Freeman, R. W. Nicholls, T. Ogawa, and P. C. Simon

INTRODUCTION

Solar energy absorbed by gases in the middle atmosphere constitutes the fundamental driver of photochemical processes and global circulation systems. The information required to describe the deposition of this energy in the atmosphere comes from studies based in the laboratory and constitutes an excellent example of the coupling between the geophysical sciences and molecular physics. The region of the solar spectrum relevant to middle atmospheric studies lies at wavelengths longer than 165-175 nm plus the hydrogen Lyman alpha line at 121.56 nm, while molecular oxygen and ozone are responsible for attenuating this energy as it penetrates the mesosphere and stratosphere. This report reviews the information presently available on the absorption cross sections of O_2 and O_3 with attention to the application of these data in middle atmospheric science. The cross sections values reported by different groups are intercompared in tabular form where feasible, and the report recommends specific values when there is a basis for preferring a particular set of results over other available data. When no such basis exists, the differences among published cross sections then serve to indicate a range of uncertainty. In these cases the report indicates the need for additional work. Specific topics addressed are the absorption of molecular oxygen at Lyman alpha, in the Schumann-Runge continuum, in the Schumann-Runge bands, and in the Herzberg continuum. For ozone, the document considers the Hartley and Huggins bands.

MOLECULAR OXYGEN

(a) The Herzberg Continuum

The Herzberg I dissociation continuum, here referred to simply as the Herzberg continuum, corresponds to the upward transition $A^3\Sigma_u^+ \leftarrow X^3\Sigma_g^-$. This transition is strictly forbidden by electric dipole selection rules, resulting in weak absorption at all wavelengths. The continuum extends from 242.4 nm to approximately 150 nm with a maximum cross section in the vicinity of 1×10^{-23} cm^2 between 195 and 200 nm. At wavelengths less than 200-210 nm the Herzberg continuum lies beneath the Schumann-Runge bands where it makes a minor contribution to the total absorption cross section. For aeronomic purposes one usually takes the term "Herzberg continuum" as synonomous with the wavelength region 200-242 nm, although this is incorrect terminology from the viewpoint of molecular physics. Absorption of solar radiation by O_2 at wavelengths from 200-242 nm constitutes the major source of atmospheric atomic oxygen below approximately 60-65 km in altitude. Opacity in this spectral range is provided by both O_2 and O_3 with the latter becoming dominant in the vicinity of 215 nm depending on altitude. Evaluation of the production rate of oxygen atoms therefore requires knowledge of both the cross section of the Herzberg continuum and the ozone Hartley bands, to be considered in a later section.

Laboratory measurements of the Herzberg continuum cross section that are relevant to this review have been reported by DITCHBURN AND YOUNG (1962), BLAKE ET AL. (1966), SHARDANAND (1969), OGAWA (1971), HASSON AND NICHOLLS (1971) and SHARDANAND AND PRASAD-RAO (1977). Experimentally determined cross sections vary linearly with pressure, an effect probably arising from dimer formation and collision-induced absorption. The measurements have been made under various conditions of pressure and absorption pathlength, and in each case the experimenters report values extrapolated to zero pressure. Table 1 summarizes the

PRECEDING PAGE BLANK NOT FILMED

Table 1. Experimental conditions employed for the measurement of absorption in the Herzberg continuum of oxygen.

	CELL LENGTH (m)	PRESSURE (atmos)	BANDWIDTH (nm)
Ditchburn and Young (1962)	5,10,30	0.2-5	-
Blake et al. (1966)	3	$\lesssim 2$	0.2
Shardanand (1969)	0.5, 1	1-20	0.25
Ogawa (1971)	6.2	$\lesssim 1.1$	0.0075
Hasson and Nicholls (1971)	33	0-0.5	0.2-1.4
	20	0-0.5	0.007
Shardanand and Prasad Rao (1977)	0.1,0.5,1,3	1-25	0.05

experimental conditions and the corresponding data appear in Figure 1 and Table 2. The total cross section shows a sharp increase for wavelengths less than 200 nm. This arises from the increasing contribution from the overlapping wings of absorption lines in the Schumann-Runge band system, so that laboratory measurements in this region do not yield the value of the Herzberg continuum cross section alone. According to the model of BLAKE (1979) there is no wavelength shorter than 186 nm where the Herzberg continuum accounts for more than 10% of the total cross section, and only measurements at wavelengths greater than 205 nm can be assumed free of contribution from the band system.

The data shown in Figure 1 range over a factor of at least two at any wavelength. There is no reason for a poor determination of the O_2 column density and transmittance in the laboratory experiments, and the main source of error must arise from other factors. Because the cross section is very small, the measurements are particularly susceptible to error arising from absorption by sample gas impurities and ozone formed from the combination of oxygen molecules with the products of dissociation, and difficulties in estimating the collision-induced absorption that produces pressure dependence in the measured cross section. Several experiments monitored the absorption near 250-260 nm. This wavelength is beyond the threshold for the Herzberg continuum and corresponds to a maximum in the absorption cross section of ozone. The absence of absorption was interpreted as an indication that ozone formation and, presumably, impurities, were not affecting the measurements.

The main cause of discrepancies between the results appears to arise from the pressure dependence in the measured cross sections. In most cases the cross section has been measured as a function of pressure, and this shows a linear dependence over a large range. The cross section has then been extrapolated to zero pressure. In the case of the data of SHARDANAND AND PRASAD RAO (1977), the required correction for pressure dependence is large and the extrapolation may have led to substantial errors. Such errors seem less likely in the data of OGAWA (1971) because of the lower pressures used. However, the cross section reported by OGAWA (1971) drops off too slowly towards long wavelengths in a region where the ozone cross section is increasing. If it is assumed that Ogawa's cell contained ozone with a mixing ratio of 3×10^{-7} then the oxygen cross section that is obtained by subtracting the ozone absorption is in very good agreement with the results of SHARDANAND AND PRASAD-RAO (1977). OGAWA (1971) makes no mention of precautions against ozone absorption although any contamination would be small for wavelengths less than 220 nm.

HASSON AND NICHOLLS (1971) used a longer pathlength and correspondingly lower pressures than other workers. They assumed the cross section to be constant for pressures less than 200 Torr and made their measurements in that region. However, there is no apparent physical basis for this assumption and their transmittance data can equally well fit a cross section of the form $\sigma = \sigma_o + \alpha p$ at all pressures, p. This leads to a significantly smaller value of σ_o than does the original method of analysis by approximately 20% and 30% at 210 nm and 215 nm, respectively. The data of DITCHBURN AND YOUNG (1962) is unique in that it was obtained by photographic detection. It is not apparent that any errors resulted from that method.

SHARDANAND (1977, 1978) has studied the absorption by O_2-N_2 mixtures and found that the cross section is described by:

$$\sigma = \sigma_o + A\, n(O_2) + B\, n(N_2)$$

where σ_o is the Herzberg continuum cross section at zero pressure, $n(O_2)$ and $n(N_2)$ are the molecular oxygen and nitrogen number densities respectively, and A and B are temperature dependent interaction constants. The values for these constants are such that at an altitude of 15 km in the stratosphere the effects

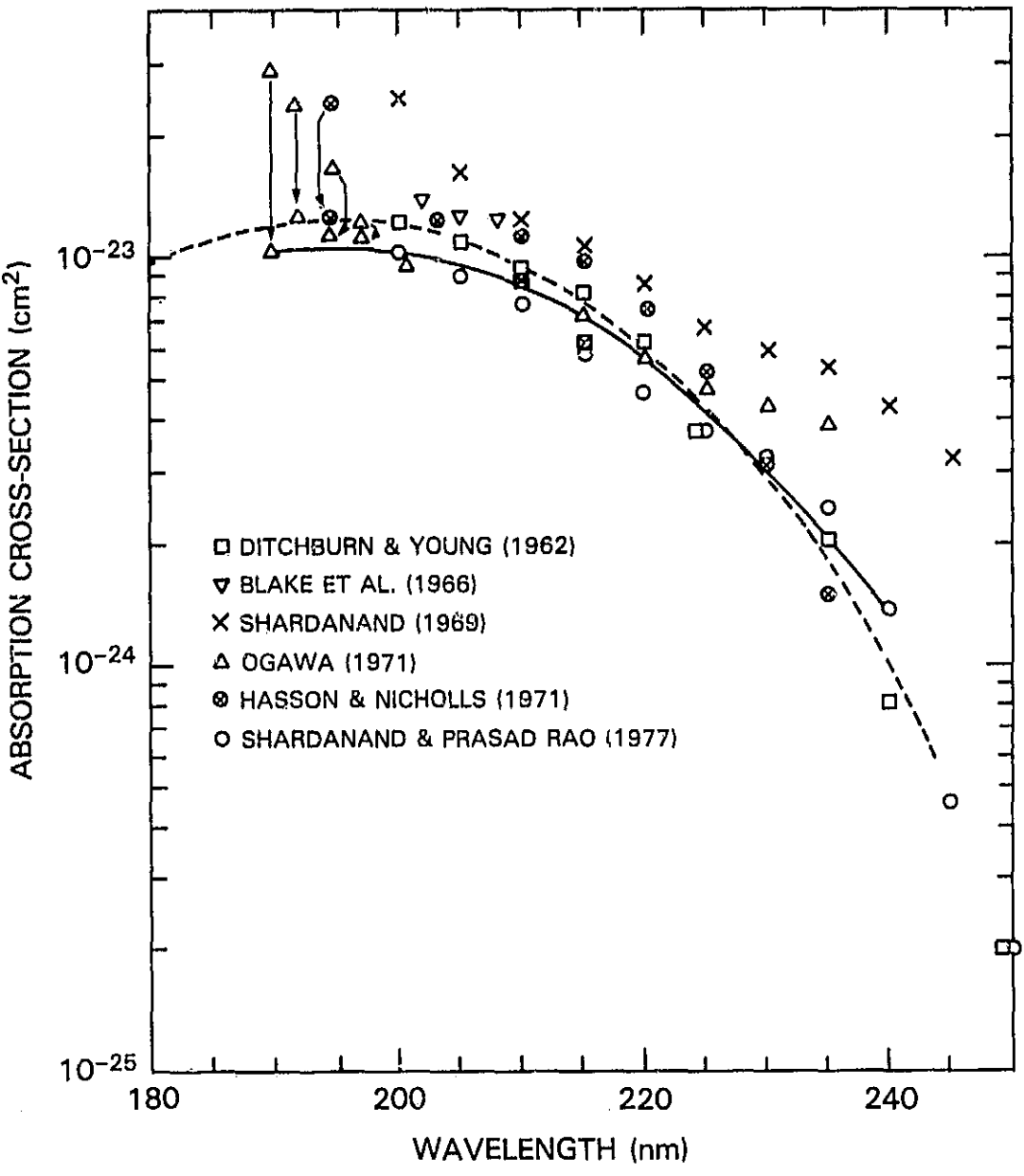

Figure 1. Laboratory measurements of the Herzberg continuum absorption cross section of molecular oxygen. The dashed line indicates theoretical results of Jarmain and Nicholls (1967). The solid line defines the recommended values.

Table 2. Laboratory determinations of the O_2 Herzberg continuum cross section (for wavelengths 200 nm and greater).

WAVELENGTH (nm)	CROSS SECTION (10^{-24} cm^2) (1)	(2)	(3)	(4)	(5)	(6)	(7)
200	12.3		24.5			10.1	
200.78				9.9			
202		14.1					
203.2					12.5		
205	10.9	13.0	16.4	9.1		8.9	
208		12.5					
210	9.3		12.7	8.05	11.2	7.7	8.7
215	8.1		10.6	7.09	0.5	5.8	6.1
220	6.1		8.5	5.65	7.3	4.6	
225	3.7		6.6	4.68	5.1	3.7	
230	3.0		5.65	4.20	3.1	3.2	
235	2.0		5.3	3.8	1.5	2.4	
240	0.8		4.2			1.4	
245			3.2			0.45	
250	0.2					0.20	

(1) Ditchburn and Young (1962)
(2) Blake et al. (1966)
(3) Shardanand (1969)
(4) Ogawa (1971)
(5) Hasson and Nicholls (1971)
(6) Shardanand and Prasad Rao (1977)
(7) Reanalysis of Hasson and Nicholls (1971) using $\sigma = \sigma_o + \alpha p$

of collision induced absorption increase the cross section by about 25% in the region 200 nm to 240 nm. The changes diminish to less than 1% above 35 km. Values for the interaction constants A and B from the data of SHARDANAND (1978) appear in Figure 2 for the temperatures 200K and 300K. Values for intermediate temperatures can be obtained by making an interpolation in terms of the logarithms of A and B.

Balloon-borne spectrometer measurements of the attenuated solar irradiance in the stratosphere allow inference of the Herzberg continuum cross section after correction for the atmospheric opacity provided by ozone. Such work, as reported by FREDERICK AND MENTALL (1982) and HERMAN AND MENTALL (1982), implies cross sections similar to or somewhat smaller than reported by SHARDANAND AND PRASAD-RAO (1977). These in situ results have the advantage of being free from the pressure dependence encountered in the laboratory. However, the inferred O_2 cross section depends sensitively on the accuracy of a simultaneous ozone measurement and of the ozone absorption cross sections required in the analysis.

It appears that many of the experimental determinations are subject to sources of error that could lead to overestimation of the Herzberg continuum cross section. In all cases, measurements at wavelengths less than 205 nm should be corrected for contributions from the Schumann-Runge band system. Perhaps the best selection from the existing laboratory data would be, the data of OGAWA (1971) for $\lambda \leq 220$ nm with those for $\lambda < 205$ nm corrected for the band contribution; the data of SHARDANAND AND PRASAD-RAO (1977); the data of HASSON AND NICHOLLS (1971) reanalyzed using the assumption that the cross section varies linearly with pressure, and the data of DITCHBURN AND YOUNG (1962). A curve fitted to these values appears in Figure 1 and constitutes the recommended cross section based on current laboratory data. New measurements of the O_2 Herzberg continuum cross section between 200 and 242 nm would make an extremely valuable contribution to our understanding of solar energy deposition in the middle atmosphere. In view of the above discussion, great care should be taken to avoid errors associated with extrapolation of laboratory results to zero pressure. Numerous measurements of the cross section are available, yet the disagreement among these results constitutes a significant uncertainty in modeling the middle atmosphere. Clearly, only a definitive determination of the cross section, which will resolve the discrepancies among previous results, is now worth performing.

(b) The Schumann-Runge Continuum of Molecular Oxygen

The strong Schumann-Runge dissociation continuum of molecular oxygen corresponds to the $B^3\Sigma_u^- \leftarrow X^3\Sigma_g^-$ transition and extends from roughly 125-130 nm up to 175 nm when one considers absorption from the $v'' = 0$ level. Thresholds for absorption from $v'' = 1$ and 2 are 180 and 185 nm, respectively, and correspond to strongly temperature dependent continuua which underlie the Schumann-Runge bands. Solar radiation at wavelengths less than 165 nm is absorbed at heights exceeding 100 km in the Earth's atmosphere, and for middle atmospheric studies one need consider the Schumann-Runge continuum cross section only at wavelengths longer than this.

The room temperature cross section in the Schumann-Runge continuum has been investigated many times. The data relevant to this review appear in Figure 3 and Table 3. Earlier data, obtained with photographic detection indicating a significantly larger cross section, have been omitted. Of the data shown, only those of GOLDSTEIN AND MASTRUP (1966) were obtained with photographic detection. The agreement between the sets of data shown is good, and if the data of METZGER AND COOK (1964) and GOLDSTEIN AND MASTRUP (1966) are excluded, it is excellent. The most probable sources of error in the measurements are gas impurities, scattered light, and pressure gauge calibration errors. All authors have used a

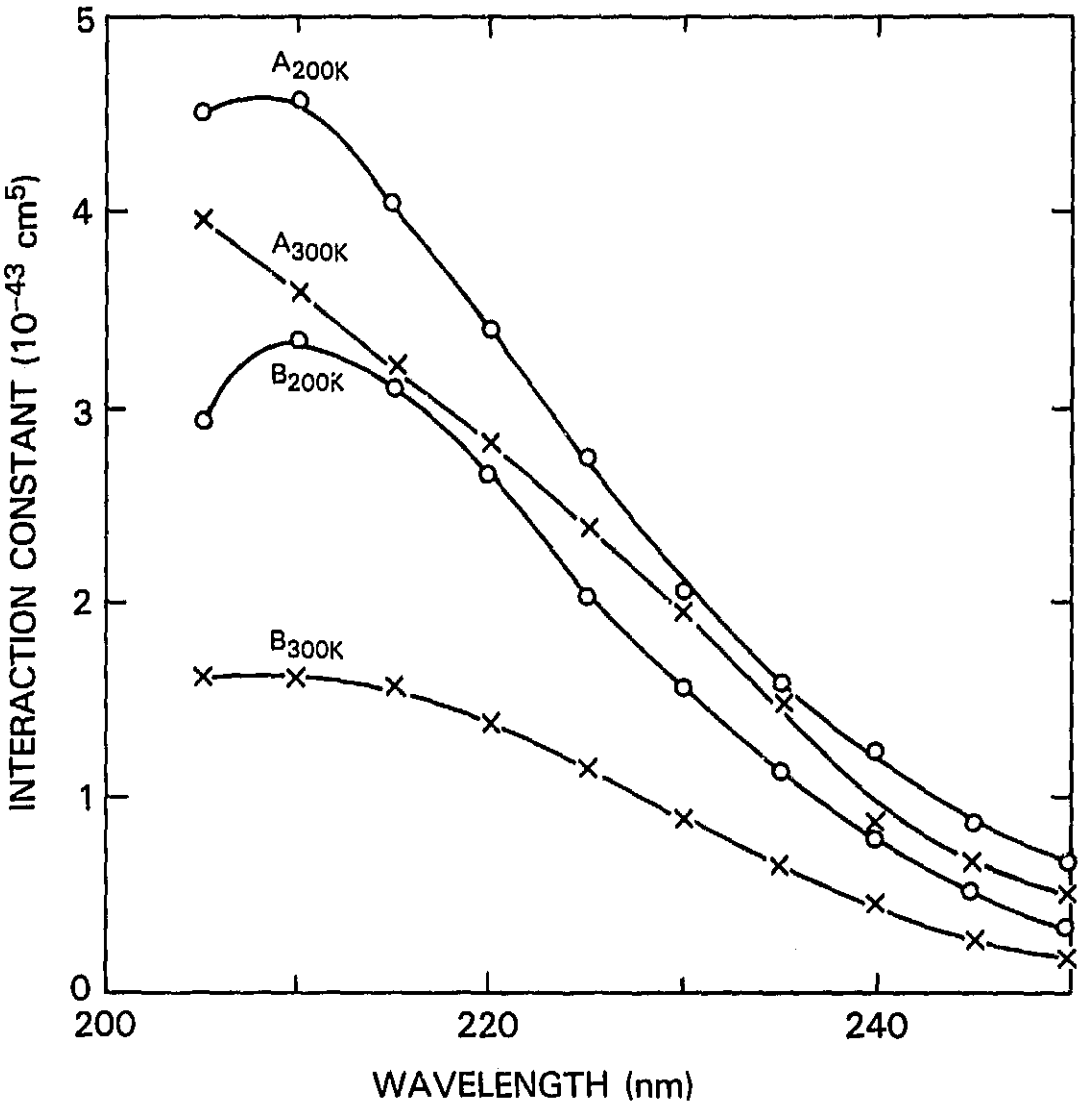

Figure 2. Temperature dependent interaction constants which describe the variation of the Herzberg continuum cross section with the atmospheric N_2 and O_2 content. Values are those derived by Shardanand (1978).

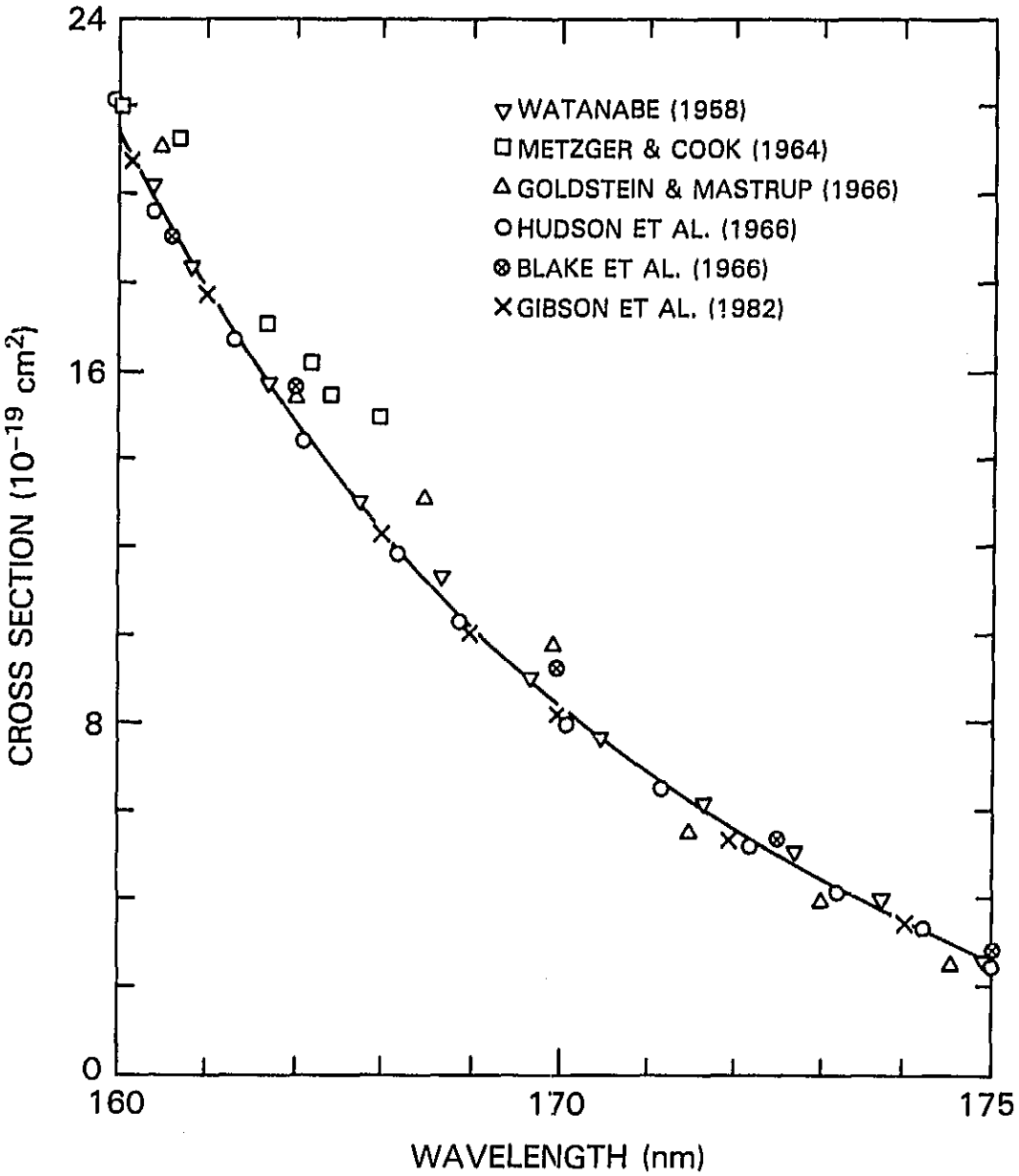

Figure 3. Laboratory measurements of the Schumann-Runge continuum cross section near the long wavelength limit. The solid line defines the recommended values.

Table 3. Laboratory determinations of the Schumann-Runge continuum cross section (for wavelengths greater than 165 nm).

λ (nm)	CROSS SECTION (10^{-19} cm^2) (1)	(2)	(3)	(4)	(5)	(6)
165		22.0			22.1	
165.10						20.76
165.4	20.1			19.6		
165.5			21			
165.6					19.0	
165.7		21.2				
165.85	18.2					
166.00						17.7
166.3				16.7		
166.7	15.6	17.0				
167.0			15.5		15.5	
167.02						14.65
167.1				14.4		
167.2		16.2				
167.4		15.4				
167.75	13.0					
168.00		15.0				12.18
168.2				11.8		
168.5			13			
168.7	11.2					
168.9				10.2		
169.00						9.96
169.7	8.92					
170.00			9.6		9.2	8.12
170.2				7.90		
170.5	7.54					
171.2				6.39		
171.5			5.4			
171.7	6.10					
172.00						5.21
172.2				5.10		
172.5					5.3	
172.7	5.06					
173.0			3.9			
173.2				4.03		
173.7	3.94					
174.00						3.27
174.2				3.21		
174.5			2.4			
174.9	2.68					
175.0				2.40	2.6	

(1) Watanabe (1958)
(2) Metzger and Cook (1964)
(3) Goldstein and Mastrup (1966)
(4) Hudson et al. (1966)
(5) Blake et al. (1966)
(6) Gibson et al. (1982)

highly pure sample gas or employed cold traps to remove condensable impurities. Most authors explicitly refer to corrections for scattered light or techniques, such as the use of narrow band detectors, to minimize its effect. The curve shown in Figure 3 is fit to the data of WATANABE (1958), HUDSON ET AL. (1966), BLAKE ET AL. (1966) and GIBSON ET AL. (1982). All except three data points are within±5% of that curve. The probable error in the curve is significantly less than 5%.

The cross section between 165 nm and 175 nm has a small temperature dependence due to absorption by molecules with rotational and vibrational excitation. Measurements in the temperature range 300K to 900K have been made by HUDSON ET AL. (1966) and in the range of 90K to 600K by GIBSON ET AL. (1982). Over the temperature range 200K to 300K, which is of interest in atmospheric applications, the temperature dependence is mainly due to redistribution of the population of rotational states. The temperature coefficient is positive in this wavelength region and according to the model and measurements of GIBSON ET AL. (1982), the cross section change over this temperature interval varies from 1.3% at 165 nm to 2.7% at 175 nm.

At wavelengths larger than 175 nm the cross section is composed of closely spaced absorption lines belonging to the Schumann-Runge band system with the underlying Schumann-Runge continuum corresponding to absorption by molecules with rotational and vibrational excitation. The absorption by this continuum tends to zero at low temperatures, but it should be included as part of the total cross section in calculations of atmospheric transmission. Values for the continuum cross section can be obtained by subtracting an estimate for the cross section due to the band system from the measured total cross section at wavelengths corresponding to absorption minima. Such measurements of the total cross section have been made by HUDSON ET AL. (1966), at temperatures of 300K, 600K and 900K, by OGAWA (1971) at room temperature, and by GIES ET AL. (1982) at 90K and 294K. Models for the continuum cross section have been given by HUDSON AND MAHLE (1972), BLAKE (1979) and GIES ET AL. (1982). In each case, the estimate for the band system contribution was obtained by summing all significant contributions from absorption lines. In practice the contribution of the Schumann-Runge continuum at wavelengths longer than 175 nm is included in temperature dependent parameterizations of radiation transfer in the Schumann-Runge bands discussed in a later section of this review.

(c) The Schumann-Runge Bands of Molecular Oxygen

The Schumann-Runge bands arise from the absorption $B\,^3\Sigma_u^- \leftarrow X\,^3\Sigma_g^-$ between 175 and 205 nm followed by predissociation yielding two $O(^3P)$ atoms. JULIENNE AND KRAUSS (1975) have discussed details of the predissociation which produces a cross section composed of numerous rotational lines. The inclusion of absorption by the Schumann-Runge bands in chemical models of the middle atmosphere has long posed formidable problems arising from the rapid variation of cross section with wavelength. Yet, consideration of the process is critical for an accurate calculation of the production rate of mesospheric atomic oxygen. Predissociation of O_2 in the Schumann-Runge bands provides the major source of oxygen atoms between approximately 60 km and 95 km in altitude. Wavelengths near the rotational line centers dominate the predissociation until such altitude as radiation coincident with the cross section maxima is depleted. At lower altitudes dissociation in the Herzberg continuum, longward of 200 nm, constitutes the largest source of atomic oxygen. However, the contribution of radiation penetrating through the wings of rotational lines in the Schumann-Runge bands is not negligible, even in the lower stratosphere (FREDERICK AND HUDSON, 1980a). At stratospheric levels, penetration of solar radiation at wavelengths in between the rotational peaks makes a substantial contribution to the dissociation of gases such as nitrous oxide and the chlorofluorocarbons. In portions of this spectral region the cross section consists of the Schumann-

Runge continuum corresponding to absorption by excited vibrational-rotational states of O_2, the Herzberg continuum, and the overlapping wings of all rotational lines in the Schumann-Runge bands. The widths of the rotational lines reflect both Doppler and predissociation broadening where the latter mechanism produces very broad wings best described theoretically by the Voigt profile. The summation of contributions from hundreds of individual rotational lines gives rise to a pseudo-continuum which can be greater than or comparable to the true continua (Herzberg, Schumann-Runge) that lie beneath the bands. Despite the complexity of this structure, an accurate treatment of the cross section is necessary for realistic predictions of the 175-200 nm radiation field at stratospheric altitudes.

A limitation inherent in much past laboratory work derives from the fact that the widths of the Schumann-Runge (SR) rotational lines are less than the instrumental resolution. Such data are not adequate for deducing cross sections directly. The direct measurement of the absolute absorption cross sections in the bands is, in principle, simple if sufficiently high spectroscopic resolution is available to render the attenuation measurements independent of the spectrometer function. In practice, direct photoelectric measurements of true cross sections in the SR bands have been reported only twice. ACKERMAN ET AL. (1970) measured the cross section at 41 discrete wavelengths, coinciding with atomic silicon lines, between 176.3 and 201.2 nm; and YOSHINO ET AL. (1982) measured the cross section of O_2 at 300K throughout the region 179.3-201.5 nm, containing the (12,0) through (1,0) bands, with a 6.65 m photoelectric scanning spectrometer possessing an instrumental width (FWHM) of 0.0013 nm. These absolute cross sections are available at wavenumber intervals of ~0.1 cm^{-1}. For cross sections greater than ~10^{-22} cm^2, i.e., for the absorption peaks of the (2,0) through (12,0) bands and for the window regions of the (7,0) through (12,0) bands, essentially all the structure observed in these cross sections is real; but for cross sections less the ~10^{-22} cm^2 some noise remains in the results, particularly in the window regions of the (v',0) bands with $v' \leq 6$, which are stratospherically important. The greatest O_2 column density used was 3.3×10^{21} cm^{-2}, and further reduction of the noise in these window regions would require the use of still greater column densities.

In the Schumann-Runge bands the width of a given rotational line depends on the Doppler width, on the predissociation line widths involved, and on the wavelength separations of neighboring individual lines (usually the triplet fine structure components) constituting the spectral feature. With respect to the instrumental width of YOSHINO ET AL. (1982), the spectral features of the Schumann-Runge bands with $v' = 1$-12 occurring in the region 201.5-179.3 nm were shown to be broad enough for the measured cross sections to be absolute in the sense of their being independent of the instrumental width, a result not achieved in recent investigations at lower resolutions (FREDERICK AND HUDSON, 1979; LEWIS ET AL., 1978, 1979, 1980; GIES ET AL., 1981). For the SR bands with $v' > 12$ the increased triplet splittings and decreased predissociation line widths produce spectral features that are narrower than the instrumental band width so that absolute cross sections have not yet been measured directly.

Laboratory studies that lack adequate spectral resolution to measure cross sections directly must infer molecular parameters from which the cross section can be computed. This procedure requires a detailed model that includes the position of all lines and their relative strengths. The quantities to be inferred from absorption data are an oscillator strength and rotational linewidth for each band. In Table 4, the recent band oscillator strengths of YOSHINO ET AL. (1982) are compared with several previous results, all of which were determined by optical techniques, except those of HUEBNER ET AL. (1975) which were obtained from electron energy loss measurements. The direct determination of Schumann-Runge band oscillator strengths, made by YOSHINO ET AL. (1982), has not been possible in previous investigations because limited

Table 4. Band oscillator strengths $f(v',o) \times 10^{-a}$ ($v' = 1$-12) of the Schumann-Runge bands of O_2.

Bandhead (nm)	v'	a	Yoshino et al. (1982)	Lewis et al. (1978-79)	Cies et al. (1981)	Frederick and Hudson (1979)	Bethke (1959)	Halmann (1966)	Ackerman et al. (1970)	Hasson et al. (1970)	Farmer et al. (1968)	Huber et al. (1975)
199.817	1	9	3.15±0.32						3.90	3.53±0.53		27.0
197.197	2	8	1.89±0.19	2.26±0.05		$2.77^{+0.07}_{-0.05}$	2.3±0.7	2.60±9.13	2.38	1.99±0.30	2.69±0.11	6.2
194.733	3	8	8.45±0.42	9.7±0.2		$7.51^{+0.13}_{-0.09}$	7.4±1.3	8.19±0.84	9.90	6.83±1.02	15.4±0.6	5.6
192.419	4	7	2.82±0.14	2.65±0.05		$3.04^{+0.02}_{-0.03}$	2.74±0.33	2.40±0.25	3.21		7.11±0.28	2.97
150.254	5	7	7.42±0.37	7.7±0.2		$7.39^{+0.90}_{-0.50}$	7.28±0.58	7.49±0.80	8.52		28.0±1.1	7.39
188.243	6	6	1.62±0.28	1.74±0.03		$1.62^{+0.05}_{-0.01}$	1.73±0.14	1.77±0.09	1.91		4.40±0.18	1.70
186.372	7	6	3.43±0.17	3.73±0.07	3.68±0.10	$3.15^{+0.10}_{-0.07}$	3.56±0.29	4.25±0.50	3.81		8.15±0.33	3.5
184.651	8	6	6.31±0.32	7.32±0.15	6.92±0.20	$5.78^{+0.04}_{-0.04}$	6.75±0.54	6.60±0.80	6.68		12.2±0.49	6.85
183.076	9	5	1.00±0.05	1.28±0.04	1.13±0.05	$1.04^{+0.36}_{-0.20}$	1.07±0.09	1.13±0.05	1.06		1.50±0.06	1.05
181.650	10	5	1.54±0.08	1.77±0.03	1.52±0.04	$1.60^{+0.47}_{-0.20}$	1.56±0.12	1.42±0.11	1.57		2.05±0.08	1.60
180.379	11	5	2.26±0.11	2.50±0.05	2.16±0.05	$1.80^{+0.53}_{-0.08}$	2.16±0.17		2.09		2.74±0.17	2.26
179.261	12	5	2.43±0.12	3.13±0.07	2.74±0.06	$2.09^{+0.08}_{-0.08}$	2.81±0.22		2.53		3.58±0.22	2.88

spectral resolution precludes the measurement of absolute integrated cross sections unless pressure broadening techniques, with their attendant uncertainties, were employed.

The most recent published determinations of the band oscillator strengths and predissociation line widths of the SR bands are those of FREDERICK AND HUDSON (1979) and the University of Adelaide group (LEWIS ET AL., 1978, 1979, 1980; GIES ET AL., 1981) who used instrumental band widths (FWHM) of 0.0075 nm ($\approx$2.3 cm^{-1}), and 0.0060 nm ($\approx$1.9 cm^{-1}), respectively. For many of the bands, significant differences exist between the band oscillator strengths and predissociation line widths obtained by these two groups, and sometimes the ranges of values defined by the quoted experimental errors do not overlap. In these recent photoabsorption studies, performed in the absence of significant pressure broadening, the quantities measured are not absolute cross sections but are ratios of incident to transmitted intensities each convolved with the instrumental function (FREDERICK AND HUDSON, 1979) or the analogous equivalent widths (LEWIS ET AL., 1978, 1979; GIES ET AL., 1981). Detailed modeling procedures are then invoked in which the cross section is computed as a function of wavenumber for rotational lines with assumed Voigt profiles, and in which the band oscillator strengths and predissociation line widths are treated as parameters which are adjusted to obtain agreement between the measured and computed instrumentally convolved intensity ratios or equivalent widths. Because band oscillator strengths and predissociation line widths may, to a considerable degree, be correlated inversely in the computed cross sections, and because line center positions calculated from imperfectly known spectroscopic constants (especially triplet splitting constants) are also required in the cross section computations, it has proven difficult to extract accurate values of band oscillator strengths and predissociation line widths by such methods. Conversely, the absolute cross sections that can be computed at arbitrarily high resolution from such band oscillator strengths and predissociation line widths are subject to uncertainties which are difficult to quantify.

We note that as a result of a systematic experimental error the values of $f(v',0)$ with $v' > 6$ found by the Australian group in 1978 (LEWIS ET AL., 1978) have been revised downwards in their most recent publication (GIES ET AL., 1981). If we consider the results of LEWIS ET AL. (1978, 1979) for $2 \leq v' \leq 6$ and those of GIES ET AL. (1981) for $12 > v' > 6$ as the best available University of Adelaide values, then the values of $f(v',0)$ of YOSHINO ET AL. (1982) lie between these results and those of FREDERICK AND HUDSON (1979) for $v' = 3$-8, 10, 12. If the errors cited in Table 4 are taken into account, it is seen that for $v' = 2$, 3, 8, and 12 neither of the ranges of $f(v',0)$ values found by these two research groups overlaps the range of values of YOSHINO ET AL. (1982), whereas for $v' = 4$, 5, 10, and 11 each of the ranges so found overlaps that of YOSHINO ET AL. (1982).

The oscillator strengths of HASSON ET AL. (1970) in Table 4 are obtained from photographic absorption measurements in air at one atmosphere in which the Schumann-Runge bands may be somewhat pressure broadened. The values of BETHKE (1959) and HALMANN (1966) are from low resolution photoelectric measurements on O_2 spectra which were pressure broadened by argon; these results agree best with those of YOSHINO ET AL. (1982) for intermediate values of v', 4 to 11, where the band overlapping effects present at high v' are small, and where the effects of the Herzberg continuum, relatively strong 'hot' bands, and possible dimer formation, which are present for bands with low v', are absent. The values of FARMER ET AL. (1968) are all much higher than those of YOSHINO ET AL. (1982), indicating a large systematic error in the low resolution study of absorption at very small optical depths (<0.03). The results of ACKERMAN ET AL. (1970), found from a spectrum computed by fitting a model cross section composed of rotational lines with assumed Lorentz profiles to the measured absolute cross sections at 41 discrete wavelengths, agree fairly well with the values of YOSHINO ET AL. (1982) for $v' \geq 8$, and the disagreement at the lowest v' values

may be due to overestimation, by ACKERMAN ET AL. (1970), of the contribution from the underlying Herzberg continuum and to the reduced accuracy of their extrapolated cross section measurements in this region.

The most recent determinations of rotational line widths for the (v',0) bands are those of FREDERICK AND HUDSON (1979) for v' = 2-13, and those of the University of Adelaide group for v' = 6-14 (LEWIS ET AL., 1981). In another paper, LEWIS ET AL. (1980) compare the results of FREDERICK AND HUDSON (1979) with the 1978 and 1979 Australian results, and conclude that there is no evidence for the increases in predissociation line widths with rotational quantum number suggested but not confirmed by FREDERICK AND HUDSON (1979). However, in the paper by GIES ET AL. (1981), the previously published mean values of the line widths determined for v' = 7-14 are revised upwards by 10-78% for v' = 7, 8, 9, 10, 13, and 14 and downwards by 4-10% for v' = 10 and 11. GIES ET AL. (1981) state that despite these revisions there is still no statistically significant variation of line width with rotational quantum number. If these revised values are accepted, there remain major disagreements with the values of FREDERICK AND HUDSON (1979). The quoted errors in the line widths of the (2,0) through (13,0) bands are in the range 5-13% in the University of Adelaide work, and are in the range 2-18% in the results of FREDERICK AND HUDSON (1979), except for the larger uncertainties of ~35% and ~55% for the (9,0) and (11,0) bands, respectively. Since the cross section in the wing of a line is roughly proportional to the line width, it is clear that the above differences would translate into large differences in cross section in window regions, and to still larger difference in the transmission of solar radiation through windows in the Schumann-Runge bands. Both research groups agree as to the existence of an overall pattern showing three maxima in predissociation line width at v' = 4, 7, 11, and this pattern is also exhibited in the theoretical work of JULIENNE (1976). At present the origin of the discrepancies among the various data sets is unknown. It would be extremely useful to infer rotational line widths from the high resolution cross sections of YOSHINO ET AL. (1982) in an attempt to resolve these problems.

(d) Absorption by Molecular Oxygen in the Vicinity of the Hydrogen Lyman Alpha Line

Absorption by molecular oxygen is primarily responsible for attenuating the intense hydrogen Lyman alpha line in the upper mesosphere. Although this process makes a negligible contribution to the destruction rate of O_2, the dissociation of water vapor by Lyman alpha radiation is a major source of hydrogen atoms and hydroxyl radicals above approximately 70 km in altitude. The O_2 absorption cross section displays large variations in the vicinity of Lyman alpha, and a deep minimum occurs near the wavelengths of the broad solar emission line. The combination of the large solar irradiance with the small cross section allows the Lyman alpha line to play a significant role in middle atmospheric processes. HUDSON (1971) reviewed the measurements available at the time of publication. Of these, only the data of OGAWA (1968) gave the cross section as a function of wavelength over the entire interval of interest. The solar Lyman alpha line has a full width at half maximum near 0.1 nm over which the O_2 cross section varies significantly. Therefore, in calculations of Lyman alpha penetration into the mesosphere it is necessary to convolve the emission line profile with the varying cross section (FREDERICK AND HUDSON, 1980; LEWIS ET AL., 1983).

The most recent investigations of the O_2 absorption cross section near Lyman alpha are those of DOSE ET AL. (1975), CARVER ET AL. (1977) and LEWIS ET AL. (1983) performed with spectral resolutions of 0.0015, 0.006, and 0.005 nm respectively. The measured cross sections are pressure dependent and require correction for aeronomic application. Only the latter two of the above studies examined temperature dependence. Near the cross section minimum the room

temperature results of all three studies are in good agreement but are approximately 15% below the corresponding values of OGAWA (1968). As one moves away from the absorption minimum, the values of LEWIS ET AL. (1983) become progressively larger than the earlier data of CARVER ET AL. (1977). For comparison purposes, Table 5 presents the values of LEWIS ET AL. (1983) for the temperatures 84, 203, and 288K together with those of CARVER ET AL. (1977) at 82, 195, and 294K. Also included are the room temperature results of OGAWA (1968). At present, the differences among the various results are unresolved. Given the discrepancies, further studies of the temperature dependence of the O_2 cross section near Lyman alpha should be undertaken. The available data show that the temperature dependence is significant, and it should be included in mesospheric calculations.

(e) The Incorporation of Cross Section Data Into Atmospheric Models: The Schumann-Runge Bands

Molecular transitions which connect a stable ground state to a continuum give rise to absorption cross sections that vary smoothly with wavelength. The use of such data in atmospheric models poses no computational or conceptual problems. One need simply choose an appropriate wavelength grid such that the variation in cross section is not extreme between adjacent values and adopt average numbers over each interval. Temperature dependence is only a minor complication, necessitating the input of several sets of cross section values and interpolation.

The Schumann-Runge bands of O_2 constitute a special case in which the absorption varies so drastically over extremely small wavelength scales that it is not feasible to simply break the spectral region into intervals and adopt average cross section values in each. The relevant quantities for model calculations are the transmission of solar radiation, T_{SR}, defined as the fraction of incident solar radiation in some wavelength interval that reaches a given altitude, and the O_2 dissociation rate, J_{SR}. For later use it is convenient to split the spectral range of the Schumann-Runge bands into "n" segments each covering a wavelength interval $\Delta\lambda(i)$, i = 1, 2,...,n. The relevant quantities are then:

$$T_{SR}(i,z,\theta) = \frac{1}{\Delta\lambda(i)} \int_{\Delta\lambda(i)} d\lambda \exp\left[-\tau_1(\lambda,z)\sec\theta\right] \qquad (1)$$

and:

$$\tilde{J}_{SR}(z,\theta) = \sum_{i=1}^{n} J_{SR}(i,z,\theta) \qquad (2)$$

where:

$$J_{SR}(i,z,\theta) = \int_{\Delta\lambda(i)} d\lambda\, \sigma_2(\lambda,z)F(\lambda)\exp[-\tau_1(\lambda,z)\sec\theta] \qquad (3)$$

In these expressions the optical depth $\tau_1(\lambda,z)$ includes contributions from both O_2 and O_3:

$$\tau_1(\lambda,z) = \tau_1(O_3,\lambda,z) + \tau_1(O_2,\lambda,z) \qquad (4)$$

Table 5. Measured values of the absorption cross section of molecular oxygen in the vicinity of Lyman alpha.

WAVELENGTH (nm)	CROSS SECTION (10^{-21} cm^2) (1)	(2)	(3)	(4)	(5)	(6)	(7)
121.46		31.9	32.7	32.3	36.3	38.1	40.3
121.47					32.3	33.6	35.2
121.48	37.2	24.9	26.0	25.3	28.7	30.2	31.4
121.49					24.6	25.9	27.4
121.50	26.2	19.6	20.8	18.2	21.8	23.1	23.5
121.51					19.4	19.9	20.1
121.52	20.2	15.0	14.2	13.5	16.9	17.7	17.4
121.53					15.1	15.4	14.9
121.54	15.2	12.2	12.5	10.6	12.8	13.1	12.9
121.55					11.6	11.3	11.7
121.56					10.4	9.7	10.3
121.563	1.13	10.52					
121.57					9.1	8.3	8.4
121.572	1.03	9.59					
121.58		9.33	7.8	7.3	9.1	8.2	7.7
121.59					8.3	7.6	7.0
121.60	9.45	8.77	6.6	6.7	8.3	6.6	6.3
121.61					8.1	6.6	5.8
121.62	9.63	9.00	6.8	5.6	8.2	6.4	5.2
121.63					8.4	6.6	5.3
121.64	10.1	9.29	7.9	5.3	8.8	6.6	5.3
121.65					9.4	7.4	5.7
121.66	11.8	10.2	77.7	6,0	10.0	7.9	6.0
121.67					10.8	8.6	6.7
121.68	13.8	12.8	9.6	6.7	12.0	9.1	7.1
121.69					13.2	10.3	8.0
121.70	16.7	14.6	10.8	8.2	14.2	11.6	9.3

(1) Ogawa (1968), room temperature
(2) Carver et al. (1977), 294K
(3) Carver et al. (1977), 195K
(4) Carver et al. (1977), 82K
(5) Lewis et al. (1983), 288K
(6) Lewis et al. (1983), 203K
(7) Lewis et al. (1983), 84K

where

$$\tau_1(O_3,\lambda,z) = \sigma_3(\lambda) \int_z^\infty dz'[O_3(z')] \quad (5)$$

and

$$\tau_1(O_2,\lambda,z) = \int_z^\infty dz' \; \sigma_2(\lambda,z')[O_2(z')] \quad (6)$$

In equations 1 through 6, z refers to altitude, θ to solar zenith angle, $\sigma_3(\lambda)$ is the absorption cross section of ozone, and $\sigma_2(\lambda,z)$ is the absorption cross section of O_2 which is temperature, and therefore altitude dependent. The O_2 cross section here includes all contributions from the Herzberg continuum, the Schumann-Runge continuum, as well as the Schumann-Runge bands. The quantities $[O_2(z)]$ and $[O_3(z)]$ denote the local number densities of molecular oxygen and ozone respectively. Note that in the wavelength interval of the Schumann-Runge bands, 175-205 nm, one may neglect temperature dependence in the ozone absorption cross section.

In practice it is adequate to assume a constant solar irradiance, F(i), and ozone cross section, $\sigma_3(i)$, over each interval $\Delta\lambda(i)$ so that the relevant expressions become

$$T_{SR}(i,z,\theta) = \frac{\exp[-\tau_1(O_3,z)\sec\theta]}{\Delta\lambda(i)} \int d\lambda \exp[-\tau_1(O_2,\lambda,z)\sec\theta] \quad (7)$$

and:

$$J_{SR}(i,z,\theta) = F(i)\exp[-\tau_1(O_3,z)\sec\theta] \int d\lambda \; \sigma_2(\lambda,z) \quad (8)$$

$$\exp[-\tau_1(O_2,\lambda,z)\sec\theta]$$

The integrals in equations 7 and 8 contain all rotational line structure of the Schumann-Runge bands and require detailed numerical evaluation. Tabulations of these integrals based on various sets of Schumann-Runge band cross section values have been published by NICOLET AND PEETERMANS (1980) and FREDERICK AND HUDSON (1980a,b). The problem is then to develop parameterizations of these results to provide relatively simple and accurate expressions for incorporation into atmospheric models. Such parameterizations have been reported by PARK (1974), NICOLET AND PEETERMANS (1980), NICOLET (1981) and ALLEN AND FREDERICK (1982). It is reasonable to adopt the slant path O_2 column content measured along the incoming solar beam as the independent variable. This neglects the fact that at various solar zenith angles slightly different temperatures, needed in evaluating the optical depth, equation 6, are associated with the same O_2 column. Variations on this approach were taken by NICOLET AND PEETERMANS (1980) and FREDERICK AND HUDSON (1980a,b). ALLEN AND FREDERICK (1982) evaluated the errors incurred in this simplification and found them to be non-negligible at optical depths greater than unity although they are probably smaller than the uncertainty in the available cross section values.

The high resolution results of YOSHINO ET AL. (1982) for a temperature of 300K have not yet been parameterized for easy incorporation into atmospheric calculations. Analysis of these data to obtain rotational line widths, when

combined with the measured oscillator strengths, would allow cross sections over a range of temperature to be generated from a detailed spectral model such as that used by FREDERICK AND HUDSON (1980a). These high resolution results could then be processed by the methods of NICOLET AND PEETERMANS (1980) or ALLEN AND FREDERICK (1982) to yield an improved parameterization of the interaction of the 175-205 nm solar radiation with atmospheric gases. Note that the detailed spectral model is required to generate cross sections at arbitrary temperatures and to compute the magnitude of the cross section in between the strong rotational lines where the values are sufficiently small, on the order of 10^{-24} to 10^{-23} cm^2, that the laboratory measurements are unable to provide accurate data.

OZONE

(a) The Hartley Bands (200-308 nm)

The spectral region from 200 nm to approximately 300-310 nm encompasses the Hartley bands which are of prime importance both in controlling the penetration of solar radiation through the atmosphere and for the measurement of middle atmospheric ozone abundances via ultraviolet absorption techniques. SIMONS ET AL. (1973) note that the total cross section in this region of the spectrum consists of at least two distinct components. In fact, the so-called Hartley "bands" consist of a smooth continuum with a weak band system imposed upon it, the former contribution being by far the dominant one. The electronic transition involved is $^1B_2 \leftarrow X^1A_1$ plus associated bending and stretching modes (SIMONS ET AL., 1973). The state of knowledge as regards cross section values for aeronomic modeling has changed little since the review of HUDSON (1971), and consequently the treatment here will be brief. A number of independent measurements of the cross section exist (INN AND TANAKA, 1953; HEARN, 1961; DEMORE AND RAPER, 1964; GRIGGS, 1968), and the overall agreement is excellent. All of these data, however, refer to room temperature. VIGROUX (1953) examined the temperature dependence of the cross section for wavelengths longward of 244.8 nm and found it to be nonnegligible in the Hartley region. At a temperature of 198K the measured cross section near 300 nm is approximately 90% of the result for 291K, while at 255 nm the corresponding value is 98%. Although these changes are not large compared with the uncertainties involved in atmospheric modeling, the reported cross section variations with temperature are greater than the error tolerable in ozone measurements if long term trends are to be detected early. In view of this, a definitive investigation of the cross section's temperature dependence below 300 nm should be performed. For use in atmospheric calculations the numbers tabulated by NICOLET (1981) are representative of the available data. Since these values are readily available in a form well-suited for aeronomic applications, this report does not reproduce the numerical results. The reader is here referred to NICOLET (1981).

(b) The Huggins Bands (308-360 nm)

A number of measurements exist in the ultraviolet region longward of 300 nm. The spectrum in this area contains the complex Huggins bands which converge to a limit near 308-309 nm. SIMONS ET AL. (1973) point out that both the Hartley region and the Huggins bands likely arise from the same electronic transition with the latter absorption corresponding to population of the ^1B state below the dissociation limit, followed by predissociation yielding O_2 and $O(^3P)$. Between the convergence limit and the region extending to roughly 315-320 nm the bands lie on top of the weak, long wavelength portion of the continuum that extends from the Hartley region. Despite the importance of the Huggins bands for the ground-based measurement of ozone, there appears to have been much less attention devoted to the fundamental molecular processes involved in this absorption than the process merits. To a great extent this reflects the increased complexity of triatomic, as opposed to diatomic, spectra.

Experimental difficulties involved in studying the Huggins bands include pressure broadening of predissociated lines and cross sections whose observed value depends on the spectral resolution of the measuring instrument. Regardless of these problems, the data of GRIGGS (1968) are in good agreement with the earlier results of INN AND TANAKA (1953). The temperature dependence of the cross section becomes significant longward of 300 nm. The standard reference here has long been the work of VIGROUX (1953), although the absolute values of GRIGGS (1968) and INN AND TANAKA (1953) are preferable at room temperature. Inspection of the data of SIMONS ET AL. (1973) for 200 and 300K gives a clear picture of the complexity of the band structure which seems to have gone unappreciated in many aeronomic applications. At discrete wavelengths between 313 and 345.5 nm VIGROUX (1953) reports cross sections that vary by less than 10% to more than a factor of 2 over the temperature range 198-291K. As shown by SIMONS ET AL. (1973), the larger variations correspond to wavelengths in between the discrete absorption peaks in the vibrational bands. The tabulation of VIGROUX (1953) does not resolve details of the spectral structure, and in many cases the cross sections reported at adjacent wavelength grid points differ by factors of 2 or more.

For modeling applications the cross section tabulation of NICOLET (1981) is adequate, even though the grid on which results are reported obscures the true spectral structure. However, the scarcity of detailed cross section data in the Huggins bands is a significant deficiency in ground based ozone measurements. Additional work, similar in complexity to that done for the Schumann-Runge bands of O_2, should be carried out here.

REFERENCES

Ackerman, M., F. Biaume and G. Kockarts (1970), Absorption cross sections of the Schumann-Runge bands of molecular oxygen, Planet. Space Sci., 18, 1639.

Allen, M. and J. E. Frederick (1982), Effective photodissociation cross sections for molecular oxygen and nitric oxide in the Schumann-Runge bands, J. Atmos. Sci., 39, 2066.

Bethke, G. W. (1959), Oscillator strengths in the far ultraviolet I. Nitric oxide, J. Chem. Phys., 31, 662.

Blake, A. J. (1979), An atmospheric absorption model for the Schumann-Runge bands of oxygen, J. Geophys. Res., 84, 1271.

Blake, A. J., J. H. Carver and G. N. Haddad (1966), Photo-absorption cross section of molecular oxygen between 1250 Å and 2350 Å, J. Quant. Spectrosc. Radiat. Transfer, 6, 451.

Carver, J. H., H. P. Gies, T. I. Hobbs, B. R. Lewis and D. G. McCoy (1977), Temperature dependence of the molecular oxygen photoabsorption cross section near the H Lyman-α line, J. Geophys. Res., 82, 1955.

Demore, W. B. and O. F. Raper (1964), Hartley band extinction coefficients of ozone in the gas phase and in liquid nitrogen, carbon monoxide and argon, J. Phys. Chem., 68, 412.

Ditchburn, R. W. and P. A. Young (1962), The absorption of molecular oxygen between 1850 and 2500 Å, J. Atmos. Terr. Phys., 24, 127.

Dose, V., U. Schmocker and G. Sele (1975), Photoabsorption coefficient of molecular oxygen in the vicinity of the hydrogen Lyman-Alpha line, Z. Phys. A., 274, 1.

Farmer, A. J., W. Fabian, B. R. Lewis, K. H. Lokan and G. N. Haddad (1968), Experimental oscillator strengths for the Schumann-Runge band system in oxygen, J. Quant. Spectrosc. Radiat. Transfer, 8, 1739.

Frederick, J. E. and R. D. Hudson (1979), Predissociation linewidths and oscillator strengths for the (2-0) to (13-0) Schumann-Runge bands of O_2, J. Mol. Spectrosc., 74, 247.

Frederick, J. E. and R. D. Hudson (1980a), Dissociation of molecular oxygen in the Schumann-Runge bands, J. Atmos. Sci., 37, 1099.

Frederick, J. E. and R. D. Hudson (1980b), Atmospheric opacity in the Schumann-Runge bands and the aeronomic dissociation of water vapor, J. Atmos. Sci., 37, 1088.

Frederick, J. E. and J. E. Mentall (1982), Solar irradiance in the stratosphere: Implications for the Herzberg continuum absorption of O_2, Geophys. Res. Lett., 9, 461.

Gibson, S. T., H. P. F. Gies, A. J. Blake, D. G. McCoy and P. J. Rogers (1983), Temperature dependence in the Schumann-Runge photoabsorption continuum of oxygen, to be published.

Gies, H. P., S. T. Gibson, D. G. McCoy, A J. Blake and B. R. Lewis (1981), Experimentally determined oscillator strengths and linewidths for the Schumann-Runge band system of molecular oxygen. III. The (7-0) to (19-0) bands, J. Quant. Spectrosc. Radiat. Transfer, 26, 469.

Gies, H. P. F., S. T. Gibson, A. J. Blake and D. G. McCoy (1982), The Schumann-Runge continuum of oxygen at wavelengths greater than 175 nm, J. Geophys. Res., 87, 8307.

Goldstein, R. and F. N. Mastrup (1966), Absorption coefficients of the O_2 Schumann-Runge continuum from 1270 Å - 1745 Å using a new continuum source, J. Opt. Soc. Am., 56, 765.

Griggs, M. (1968), Absorption coefficient of ozone in the ultraviolet and visible regions, J. Chem. Phys., 49, 857.

Halmann, M. (1966), Isotope effects on Franck-Condon factors. IV. Pressure-broadened absorption intensities of the Schumann-Runge bands of $^{16}O_2$ and $^{18}O_2$, J. Chem. Phys., 44, 2406.

Hasson, V. and R. W. Nicholls (1971), Absolute spectral absorption measurements in molecular oxygen from 2640 - 1920 Å: II. Continuum measurements 2430 - 1920 Å, J. Phys. B: Atom. Mol. Phys., 4, 1789.

Hasson, V., G. R. Hebert and R. W. Nicholls (1970), Measured transition probabilities for bands of the Schumann-Runge ($B^3\Sigma_u^- - X^3\Sigma_g^-$) band system of molecular oxygen, J. Phys. B: Atom. and Molec. Phys., 3, 1188.

Hearn, A. G. (1961), The absorption of ozone in the ultraviolet and visible regions of the spectrum, Proc. Phys. Soc. London, 78, 932.

Herman, J. R. and J. E. Mentall (1982), O_2 absorption cross sections (187-225 nm) from stratospheric solar flux measurements, J. Geophys. Res., 87, 8967.

Hudson, R. D. (1971), Critical review of ultraviolet photoabsorption cross sections for molecules of astrophysical and aeronomic interest, Rev. Geophys. Space Phys., 9, 305.

Hudson, R. D. and S. H. Mahle (1972), Photodissociation rates of molecular oxygen in the mesosphere and lower thermosphere, J. Geophys. Res., 77, 2902.

Hudson, R. D., V. L. Carter and J. A. Stein (1966), An investigation of the effect of temperature on the Schumann-Runge absorption continuum of oxygen, 1580 Å - 1950 Å, J. Geophys. Res., 71, 2295.

Hueber, R. H., R. J. Cellota, S. R. Mielczarek and C. E. Kuyatt (1975), Apparent oscillator strengths for molecular oxygen derived from electron energy loss measurements, J. Chem. Phys., 63, 241.

Inn, E. C. Y. and Y. Tanaka (1953), Absorption coefficient of ozone in the ultraviolet and visible regions, J. Optical Soc. Amer., 45, 870.

Jarmain, W. R. and R. W. Nicholls (1967), A theoretical study of the v" = 0, 1, 2 progressions of bands and adjoining photodissociation continua of the O_2 Herzberg I system, Proc. Phys. Soc., 90, 545.

Julienne, P. S. (1976), $^3\Sigma_u^- - {}^3\Sigma_u^+$ coupling in the O_2 $B^3\Sigma_u^-$ predissociation, J. Mol. Spectrosc., 63, 60.

Julienne, P. S. and M. Krauss (1975), Predissociation of the Schumann-Runge bands of O_2, J. Mol. Spectrosc., 56, 270.

Lewis, B. R., J. H. Carver, T. I. Hobbs, D. G. McCoy and H. P. Gies (1978), Experimentally determined oscillator strengths and line widths for the Schumann-Runge band system of molecular oxygen. I. The (6-0) - (14-0) bands, J. Quant. Spectrosc. Radiat. Transfer, 20, 191.

Lewis, B. R., J. H. Carver, T. I. Hobbs, D. G. McCoy and H. P. Gies (1979), Experimentally determined oscillator strengths and line widths for the Schumann-Runge band system for molecular oxygen. II. The (2-0) - (5-0) bands, J. Quant. Spectrosc. Radiat. Transfer, 22, 213.

Lewis, B. R., J. H. Carver, T. I. Hobbs, D. G. McCoy and H. P. Gies (1980), Rotational variation of predissociation linewidths for the Schumann-Runge bands of molecular oxygen, J. Quant. Spectrosc. Radiat. Transfer, 24, 365.

Lewis, B. R., I. M. Vardavas and J. H. Carver (1983), The aeronomic dissociation of water vapour by solar H Lyman alpha radiation, J. Geophys. Res., 88, 4935.

Metzger, P. H. and G. R. Cook (1964), A re-investigation of the absorption cross sections of molecular oxygen in the 1060 Å - 1800 Å region, J. Quant. Spectrosc. Radiat. Transfer, 4, 107.

Nicolet, M. (1981), The solar spectral irradiance and its action in the atmospheric photodissociation processes, Planet. Space Sci., 29, 951.

Nicolet, M. and W. Peetermans (1980), Atmospheric absorption in the O_2 Schumann-Runge band spectral range and photodissociation rates in the stratosphere and mesosphere, Planet. Space Sci., 28, 85.

Ogawa, M. (1968), Absorption coefficients of O_2 at the Lyman alpha line and its vicinity, J. Geophys. Res., 73, 6759.

Ogawa, M. (1971), Absorption cross sections of O_2 and CO_2 continua in the Schumann and far-UV regions, J. Chem. Phys., 54, 2550.

Park, J. H. (1974), The equivalent mean absorption cross sections for the Schumann-Runge bands: Application to the H_2O and NO photodissociation rates, J. Atmos. Sci., 31, 1893.

Shardanand (1969), Absorption cross sections of O_2 and O_4 between 2000 and 2800 Å, Phys. Rev., 186, 5.

Shardanand (1977), Nitrogen-induced absorption of oxygen in the Herzberg continuum, J. Quant. Spectrosc. Radiat. Transfer, 18, 525.

Shardanand (1978), Temperature effect on the nitrogen induced absorption of oxygen in the Herzberg continuum, J. Quant. Spectrosc. Radiat. Transfer, 20, 265.

Shardanand and A. D. Prasad-Rao (1977), Collision induced absorption of O_2 in the Herzberg continuum, J. Quant. Spectrosc. Radiat. Transfer, 17, 433.

Simons, J. W., R. J. Paur, H. A. Webster III and E. J. Bair (1973), Ozone ultraviolet photolysis. VI. The ultraviolet spectrum, J. Chem. Phys., 59, 1203.

Vigroux, E. (1953), Contribution a l'estude experimentale de l'absorption de l'ozone, Ann, Phys., 8, 709.

Watanabe, K. (1958), Ultraviolet absorption processes in the upper atmosphere, Adv. Geophys., 5, 153.

Yoshino, K., D. E. Freeman, J. R. Esmond and W. H. Parkinson (1983), High resolution absorption cross section measurements and band oscillator strengths of the (1,0), (12,0) Schumann-Runge bands of O_2, Planet. Space Sci., 31, 339.

OMIT 70
LAST

CZECHOSLOVAK ACTIVITY IN MAP

J. Lastovicka

The Czechoslovak national MAP program consists of 7 scientific sub-programs:

(1) Disturbances of the atmosphere at heights of 120 to 40 km by penetration of meteoroids of metre and decimetre dimensions, - Dr. Ceplecha (Astronomical Institute, Czechosl. Acad. Sci., Ondrejov):

Continuous photographic observations of fireballs were performed at 17 stations in Czechoslovakia, 23 stations in FRG, 3 stations in Holland and 2 stations in Austria, and yielded multistational records of 38 fireballs during the year 1982. Results on the most significant of them (9 fireballs) have already been published in the SEAN Bulletin: 4 fireballs penetrated the whole middle atmosphere. These observations are coordinated and evaluated by the Astronomical Institute in Ondrejov.

A new theoretical approach to the basic equations of meteoroid penetration through the atmosphere yielded solutions for any atmospheric model given in a quite general form. The assumption of a simple atmospheric model for deep-penetrating fireballs yields greater values of ablation coefficients, smaller initial velocities and smaller bulk densities of meteoriods than the actual ones. The air density profile of the instant atmosphere must be used for any future work on fireballs. The average ablation coefficient and air density profile along the fireball trajectory are closely related and one determines the other.

This sub-program belongs to GLOBMET. Another sub-program belonging to GLOBMET is under preparation.

(2) Winter anomaly - Dr. Lastovicka (Geophysical Institute, Czechosl. Acad. Sci., Prague):

On the basis of 23 years of A3 absorption measurements at the Panska Ves Observatory, the major stratospheric warmings and related changes in the prevailing zonal wind in the upper mesopause region have been found to decrease, not increase, radio wave absorption (break-down of winter anomaly). The winter of 1982/83 was strongly affected by very high geomagnetic activity. The winter anomaly itself appeared to be medium or weak during this winter.

(3) Aeronomic studies with the use of ground-based measurements of radio wave propagation - Dr. Lastovicka (Geophysical Institute, Czechosl. Acad. Sci., Prague):

Nitric oxide concentration, estimated by comparing empirically derived ratios of Lyman-α and X-ray contributions to the total radio-wave absorption at 2775 kHz (A3 method; summers of 1969, 1970, 1972) with model ratios, was found to be about 8.5×10^{13} m^{-3} at 90 km and 6.5×10^{13} m^{-3} at 78 km (high values, but within the broad range of experimental values).

The Lyman-α radiation dominates in radio wave absorption on 1539 kHz (summers of 1978-1980) under non-flare conditions. The contribution of X-rays to the total absorption is about 10%. A dependence of absorption on Lyman-α and X-ray flux was derived in the form $L = A F_{\alpha}^{m} + B F_{X}^{m} + C$, where $m \in \langle 0.45 - 1.1 \rangle$ for uncorrected Lyman-α data and $m \in \langle 0.45 - 0.8 \rangle$ for corrected Lyman-α data.

(4) The interplanetary magnetic field effects in the ionosphere and atmosphere - Dr. Lastovicka (Geophysical Institute, Czechosl. Acad. Sci., Prague):

The effects of the IMF sector structure in the midlatitude ionosphere have been found to be developed better for "proton" sector boundaries (boundaries followed by streams of low-energy solar protons) than for normal sector boundaries in winter as well as at equinox, in day-time as well as at night. Equinoctial results are preliminary due to the small number of data.

(5) The geomagnetic activity influence on the troposphere, climate and weather - Dr. Bucha (Geophysical Institute, Czechosl. Acad. Sci., Prague):

Using processed sets of geomagnetic and meteorological data, it was demonstrated that increased corpuscular radiation indicated by geomagnetic activity and characterized by enhanced penetration of electrons into the middle atmosphere, by generating bremmstrahlung and forming ion clusters at altitudes of around 15 km, results in increased temperatures and atmospheric pressure in the stratosphere and troposphere. These effects also cause an immediate increase in temperature and pressure at the 500 mb level in the auroral oval and meridional-type atmospheric circulation to change to zonal. The results indicate that these changes in flow cause pronounced changes in temperature and pressure in Europe and North America and are responsible for sudden penetrations of Arctic air under decreased corpuscular radiation and for sudden stratospheric warmings under increased corpuscular radiation.

(6) Airglow variations - Dr. Rybansky (Astronomical Institute, Slovak Acad. Sci., Tatranska Lomnica):

A photometer is operating under laboratory conditions and is now being tested. The methodology of measurements and data evaluation has been improved.

(7) The dynamics of penetration of convective clouds into the stratosphere - Dr. Podhorsky (Hydrometeorological Institute, Bratislava):

A meteosys/db databank system was designed and computer programs prepared for operational evaluation of satellite and radar information in the region of Central Europe using a special uniform cartographic system. A method was developed of synchronous automated observations of upper boundaries of convective clouds with the use of geostationary and polar satellites and meteorological radars. Experiments are planned in 1983-1984.